CHALMERS
UNIVERSITY OF TECHNOLOGY

Aerodynamic study of vehicle mounted cargo boxes

A comparative study between roof boxes and tow bar mounted cargo boxes using CFD

Master’s thesis in Sustainable Energy Systems

Marcus Sandberg

DEPARTMENT OF MECHANICS AND MARITIME SCIENCES

CHALMERS UNIVERSITY OF TECHNOLOGY
Gothenburg, Sweden 2022
www.chalmers.se

MASTER’S THESIS IN SUSTAINABLE ENERGY SYSTEMS

Aerodynamic study of vehicle mounted cargo boxes

A comparative study between roof boxes and tow bar mounted cargo boxes using CFD

Marcus Sandberg

Department of Mechanics and Maritime Sciences
Division of *Vehicle Engineering and Autonomous Systems*
CHALMERS UNIVERSITY OF TECHNOLOGY
Göteborg, Sweden 2022

Aerodynamic study of vehicle mounted cargo boxes
A comparative study between roof boxes and tow bar mounted cargo boxes using CFD
Marcus Sandberg

Master's Thesis 2022:03
Department of Mechanics and Maritime Sciences
Division of Vehicle Engineering and Autonomous Systems
Chalmers University of Technology
SE-412 96 Göteborg
Sweden
Telephone: + 46 (0)31-772 1000

Cover:
Overview of the three test objects in the master thesis, the DrivAer Notchback with a roof box or an IXTAbox.

Department of Mechanics and Maritime Sciences
Göteborg, Sweden 2022-01-31

Aerodynamic study of vehicle mounted cargo boxes
A comparative study between roof boxes and tow bar mounted cargo boxes using CFD
Master's thesis in Sustainable Energy Systems
MARCUS SANDBERG
Department of Mechanics and Maritime Sciences
Division of Vehicle Engineering and Autonomous Systems
Chalmers University of Technology

Abstract

Ever rising CO_2 emission needs to be mitigated and there are many ways forward. For the car industry the way forward spells ever increasing energy efficiency and the introduction of electric vehicles. When extra cargo capacity is required for a passenger vehicle, it is common to install a roof box, for example if one is ought to go skiing. However energy efficiency, electric vehicles and roof boxes does not go hand in hand and compared to vehicle producers, and it is rare to optimise the box with a thorough aerodynamic study due to its investment cost. Initial literature surveys indicate that a substantial power increase is required, as stated C_d values are in the range of 30% increased compared to the car alone. Furthermore the frontal area is increased, increasing the power requirements even further.

The IXTAbox is a recent innovation to combat the shortfall of the roof box through putting the box on the tow bar, rather than the roof. As it lies in the wake of the vehicle it is expected that the required power increase is significantly lower compared to a roof box as no added area is done, and C_d should have a minimal impact as it lies in the wake. But it is not possible to answer how much the drag increase, and what areas of the IXTAbox is sensitive to change, which is why this thesis is conducted. To answer the questions at hand, Computational Fluid Dynamics (CFD) shall be used. With CFD, this thesis has studied and presented C_dA values for two roof box models, furthermore six IXTAboxes has been studied, and finally aerodynamic improvements to the IXTAbox has been shown. From the study, it has been seen that a roof box can increase C_dA by almost 40% while the IXTAbox increase the C_dA by 4-11% depending on its size. Finally, the important flow features when implementing the IXTAbox include that the base pressure on the trunk of the car increases compared to when only simulating the car. On the other hand, an additional stagnation point occur as the IXTAbox captures the flow coming from the underbody, essentially removing the function of the car's diffusor. With that in mind, the most successful design improvements on the IXTAbox + car achieved a lower C_dA value than the car on its own, making it a very interesting innovation to study further as it mitigates the shortfall of the roof box, heavily increased power requirements.

Keywords: Aerodynamics, vehicles, cargo boxes, roof boxes, CFD, drag, drag reduction, pressure recovery, fluid mechanics

Preface

To finalize five years engineering studies, this thesis of 30 ECTS has been performed together with Basework AB, the company behind IXTAbox. The thesis has been conducted from September 2021 to January 2022.

During the thesis I've gained a lot of new knowledge in a field of fluid mechanics I am not too familiar with, coming from chemical and energy engineering, with that in mind I would like to thank my supervisor and examiner Simone Sebben from whom I have been able to learn so much from. Furthermore I would like to thank Alexey Vdovin for aiding me with the tutorials, CAD models and computational resources at Chalmers required for the thesis.

Furthermore the thesis has provided me a great mentor to my future endeavours, Carl Rietz with whom I had many interesting talks to as we've discussed everything to IXTAboxes to entrepreneurship to which I'm very happy. With that in mind thank you all who has shared a part in this work!

Nomenclature

Abbreviations

CFD	Computational Fluid Dynamics
DES	Detached Eddy Simulation
DNS	Direct Numerical Simulation
LES	Large Eddy Simulation
RANS	Reynolds Average Navier Stoke
RKE	Realizable $K-\epsilon$ turbulence model
$K-\omega$	$K-\omega SST$ turbulence model

Symbols

Φ	Arbitrary Flow quantity
ρ	Density
τ_{ij}	Stress Tensor
t	Temporal Variable
x	Spatial Variable
δ_{ij}	Kronecker Delta
μ	Dynamic Viscosity
ν_T	Turbulent Viscosity
F	Force
F_d	Total Drag Force
A_p	Maximum projected Area
A_s	Surface Area
C_d	Drag Coefficient
C_f	Skin Friction Coefficient
C_p	Pressure coefficient
C_{ptot}	Total pressure coefficient
g_i	Gravitational source term
k	Turbulent Kinetic Energy
l	Length
M	Momentum
Re	Reynolds number
Re_x	Local Reynolds Number
U	Velocity
P	Pressure

Contents

Abstract i

Preface iii

Nomenclature v

Contents vii

1 Introduction 1
1.1 Problem Statement 1
1.2 Objectives 1
1.3 Limitations 1

2 Theory 2
2.1 Fluid Dynamics 2
2.1.1 Flow with a Pressure Gradient 2
2.2 Turbulence 3
2.3 Numerical stability when modelling road vehicles. 5
2.4 Sources of Drag 6
2.4.1 Friction Drag 6
2.4.2 Drag due to flow separation 6
2.4.3 Wake Drag 6

3 Literature Study 8
3.1 Aerodynamic devices 8
3.1.1 Passenger Cars 8
3.1.2 Trucks 8
3.2 Roof boxes 9

4 Method 10
4.1 Test Object 10
4.2 CAD drawings of IXTAbox and roof box 11
4.3 Computational domain and numerical setup 13
4.4 Mesh generation 14
4.4.1 Surface Mesh 14
4.4.2 Prism Layers and Y+ 15
4.4.3 Volume Mesh 16
4.5 Convergence criterion 16

5 Results 18
5.1 Reference: Drivaer notchback 18
5.2 Reference: Roof boxes 20
5.3 Reference: IXTAboxes 23
5.3.1 170-40 using RKE and $k - \omega$ 23
5.3.2 Boxes of height 60 26
5.3.3 Boxes of Height 40 29
5.4 Failure of RKE to predict the flow for the large boxes 32
5.5 Height Variations of Ixtabox 33
5.6 IXTAbox aerodynamic improvements on the 170-40 box 34
5.6.1 Diffusor Extension L 36
5.6.2 Diffusor Extension S 38
5.6.3 Vortex Stabiliser 40
5.6.4 Arc Diffusor 42

6 Discussion **45**

7 Conclusions **47**

References **48**
Appendix 49

1 Introduction

Carbon dioxide emissions are rising worldwide, and needs to be mitigated. For the car industry this means increased energy efficiency and a move to electric vehicles. To aid electric vehicles to move from the early adopter's phase to gaining acceptance with the early majority, more needs to be done to the ownership experience. When it comes to cargo capacity, it is common to install a roof box, for example, if one is ought to go skiing. However, this increase the aerodynamic drag by increasing the projected area of the car and increasing the drag coefficient as more losses are induced from the larger wake. Furthermore, many electric vehicles come without support to install a roof box due to the large reduction of range, due to increased drag. Cargo boxes have not been a topic of much research or discussion. However, with increased awareness of CO_2 emissions, and the entrance of electric vehicles to the market, it is one area where a little bit of innovation and thinking outside the box could go a long way. One such innovation could be the IXTAbox, a tow bar mounted cargo box with enough space to put skis and luggage in. As it connects to the tow bar, it lies in the wake, hidden by the car, one can conclude without any study that the IXTAbox will have a lower impact on drag than a roof box.

1.1 Problem Statement

Putting the extra cargo capacity on the tow bar instead of on the roof can without any Computational Fluid Dynamic (CFD) study be said to have a lower power increase compared to putting the cargo capacity on the roof, as both the projected area is decreased and no new wake volumes is formed as it would for a roof box in the mean stream. However, how much will the IXTAbox increase the drag? What are the areas of improvement on the IXTAbox? To answer those two questions, a study needs to be carried out using CFD which forms the problem for this thesis to solve.

1.2 Objectives

With previous sections in mind, this thesis will study the aerodynamic performance of six existing IXTAboxes, impact on the wake shall be studied and C_dA will be reported for each box. To compare the IXTAboxes, two roof boxes shall also be created, to study their wake, and especially have a comparison of C_dA. Finally aerodynamic improvements shall be done on the IXTAbox to map sensitive sections to C_dA so that the constructor can make well informed choices if the design is going to be improved in the future. Finally, it should be said that no literature of good quality exists for neither roof boxes, or IXTAboxes. The numerical quality of this thesis is based on the car model DrivAer notchback, whose C_dA numbers and wake structures can be compared to literature.

1.3 Limitations

As the thesis is only 20 weeks done by one student, some limitations exist and are noted below:

- No consideration to the influence of side winds are done
- Reynolds-averaged Navier Stokes(RANS) models only implicating steady state.
- Computational Resources constrained to a 20 core CPU 256 GB ram computer
- No validation to wind tunnel measuring C_d or real life driving measuring energy consumption.
- Only the vehicle model *DrivAer notchback* was used, different cars will produce different results.

2 Theory

The theory chapter in this thesis shall discuss the physics of interest to solve the problem at hand, while theory of engineering nature is left to the literature study.

2.1 Fluid Dynamics

The governing equations for CFD are the Navier Stokes equations for continuity, energy and momentum, however as no heat transfer is done, only the continuity and momentum equations are used given below as equation 2.1 and 2.2. As the gas velocity is well below the compressible range for this thesis, the density is moved out of the partial derivatives and seen as constant.

$$\rho\frac{\partial U_j}{\partial x_j} = 0 \tag{2.1}$$

$$\frac{\partial U_i}{\partial t} + U_j\frac{\partial U_i}{\partial x_j} = -\frac{\partial P}{\rho\partial x_i} + \frac{\partial \tau_{ij}}{\rho\partial xj} + g_i \tag{2.2}$$

2.1.1 Flow with a Pressure Gradient

∇P plays an important role as flow with a pressure gradient can cause flow separation, which in aerodynamics is undesirable. At the boundary, with the no-slip condition, using theory for the flat plate $v_x = v_y = 0$ for $y = 0$ thus we obtain equation 2.3 which describe the curvature of the velocity profile to the pressure gradient[1].

$$\mu\frac{\partial^2 U_x}{\partial y^2}\bigg|_{y=0} = \frac{dP}{dx} \tag{2.3}$$

For a case when $\frac{dP}{dx} = 0$ it is known that the velocity profile must be linear from the laws of calculus. Furthermore, using the laws governing calculus, much information can be gained on the physics of boundary layer separation. As the velocity is decreasing further away from the wall, but still inside the boundary layer, to eventually reach the velocity magnitude in the mean stream, the second derivative has to be negative as the velocity gradient is decreasing, this is true no matter which sign $\frac{dP}{dx}$ have. A negative pressure gradient produces a curved velocity profile down to the wall but is relatively similar to the case of $\frac{dP}{dx} = 0$.

For a positive value on $\frac{dP}{dx}$, it is noted that the second derivative $\frac{\partial^2 U_X}{\partial y^2}$ must also be positive approaching the wall. However, it has been stated that the second derivative also approaches zero from the negative side further away from the wall as the velocity gradient is continuously decreasing to the mean flow values outside the boundary layer. This means that somewhere on the interval when $\frac{dP}{dx} > 0$, there exist an inflection point in the velocity profile. As this inflection point is located in the velocity profile, it can be concluded that potentially, closest to the wall, the flow can go in negative x directions. Further out in the profile, the velocity goes in the positive x-direction. Transition phenomena is shown in figure 2.1

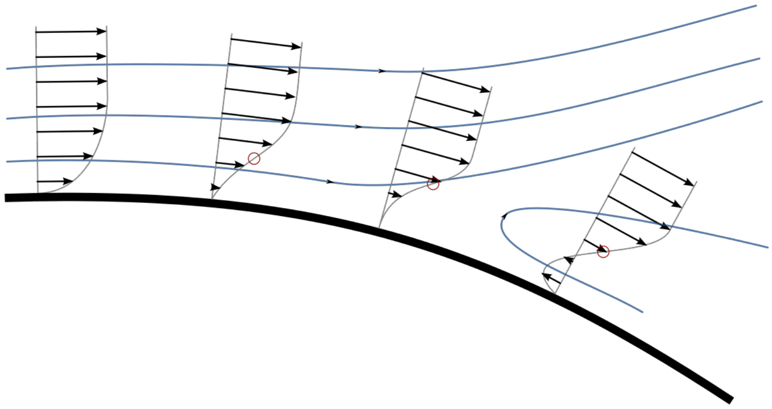

Figure 2.1: *Velocity profile development for an adverse pressure gradient, the red dot indicate the inflection point. [2]*

From the book *Fundementals of Momentum, Heat and Mass transfer by Welty et.al*, it is said that a positive $\frac{dP}{dx}$ is necessary for flow separation, but not sufficient, the negative pressure gradient is also frequently called adverse pressure gradient, which will be used further down in this thesis [1]. A negative value on $\frac{dP}{dx}$ however, cannot cause flow separation other than for sharp corners and can be said to be a favourable ∇P as it balances the growth of the boundary layer with increasing pressure.

2.2 Turbulence

In a fluid flow, when turbulence is prevalent, one can make some conclusions on the properties by just looking at the flow. First of all, chaos is observed, furthermore one can see how large vortices are broken up into smaller vortices, moreover the further away from the source of turbulence, the less chaotic the flow appears. Thus the first conclusion from observing turbulence is that decay plays a role, which is denoted as the energy cascade of turbulence and is visualised in figure 2.2

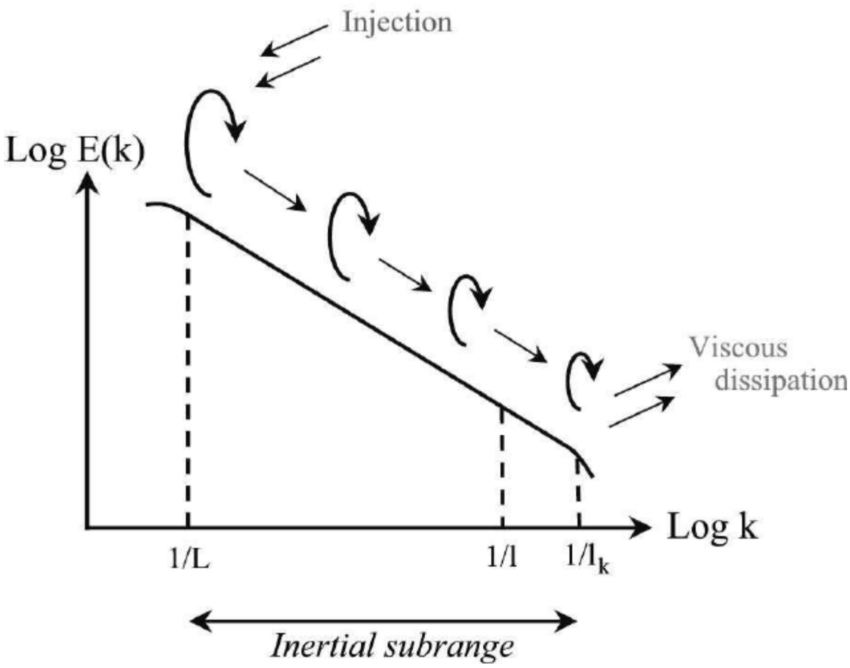

Figure 2.2: *Energy cascade of turbulence where the distinct phases of turbulence is visualised[3].*

Furthermore, one can assign several qualities to turbulent flow, such as is done in the book *Computational Fluid Dynamics for Engineers by Andersson et. al* which is cited below:

1. Irregularity - Turbulent flows are irregular, random and chaotic where the largest scales are bounded by geometry while the smallest scales are bounded by viscosity[4].
2. Diffusive - Turbulence is diffusive due to its 3-D chaotic motion and is several order of magnitude higher than molecular diffusion [4].
3. Unstable - turbulence arise due to instabilities at high enough Reynolds numbers[4].
4. 3-D structures - Turbulence is a 3-D phenomena, as mechanisms such as vortex stretching and vortex tilting can not occur in less than all the spatial dimensions. However, one could statistically model 2-D turbulence in a CFD software[4].
5. Dissipation of turbulent kinetic energy - As seen in figure 2.2 there is a flux of energy transferred from the large scales to the small scales - however, it is only at the smallest scales that losses occur, e.g. kinetic energy to heat through viscous stress. At larger length scales, the energy cascade is said to be ideal as no loss to heat occurs[4].
6. Continuum - Turbulence is a continuum phenomena where even the smallest length scales are much larger than molecular scales[4].
7. Turbulent flows are flows - Turbulence is only a feature of the flow, all fluids are turbulent at high enough Reynolds numbers[4].

Even while the smallest length scales of turbulence are of several magnitudes higher than molecular scale, they are still too small to model in CFD applications with the computer power of today. That type of simulation is called Direct Numerical Simulation (DNS) and is only done on elementary geometries with large computer clusters. To combat the cost of DNS, one can also use Large Eddy Simulation (LES), which is gaining traction in both academia and industry. In LES, one filters out the smallest length scales which are the most costly while simulating the larger length scales so that its dynamics are captured. Thus LES is always in 3-D and uses a transient solver. The RANS models are the last way to be discussed and what is applied to this thesis. The basis for the RANS models is that they separate flow variables into two parts, a mean part and a fluctuating part, such as is seen in equation 2.4 where the quantities given is an arbitrary flow variable.

$$\Phi_i = \langle \Phi_i \rangle + \phi_i \tag{2.4}$$

With this type of decomposition called Reynolds decomposition, the flow is statistically described. It does not capture the chaotic motion of turbulence in the same way that DES/LES/DNS can, which is shown in figure 2.3 to give an example.

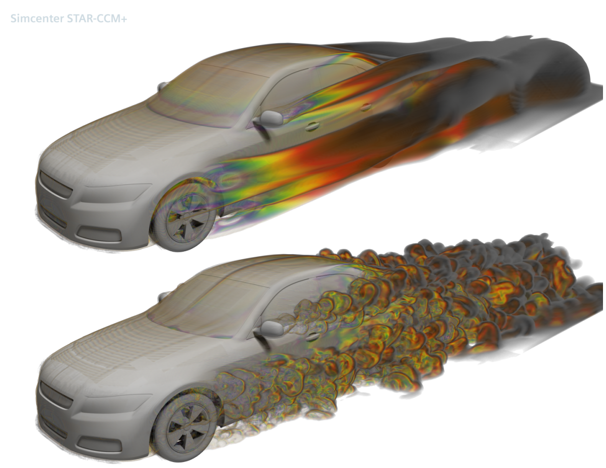

Figure 2.3: *Comparison between an unsteady RANS simulation and detached eddy simulation which show how the RANS model average the solution while the DES/LES/DNS simulations capture the chaotic motion of turbulence at various length scales.[5]*

The decomposition is then inserted into the Navier-Stokes equations where equation 2.1 and 2.2 become equation 2.5 and 2.6

$$\frac{\partial(\langle U_i\rangle + u_i)}{\partial x_i} = 0 \tag{2.5}$$

$$\frac{\partial(\langle U_i\rangle + u_i)}{\partial t} + (\langle U_i\rangle + u_i)\frac{\partial(\langle U_i\rangle + u_i)}{\partial x_j} = \frac{-1}{\rho}\frac{\partial(\langle P\rangle + p)}{\partial x_i} + \nu\frac{\partial^2(\langle U_i\rangle + u_i)}{\partial x_j \partial x_j} \tag{2.6}$$

When averaging linear terms of fluctuating variables, they become zero and thus equation 2.5 and 2.6 can be reduced to the general form of the RANS equation as seen in equation 2.7

$$\frac{\partial\langle U_i\rangle}{\partial t} + \langle U_j\rangle\frac{\partial\langle U_i\rangle}{\partial x_j} = \frac{-1}{\rho}\frac{\partial}{\partial x_j}\Big\{\langle P\rangle\delta_{ij} + \mu\Big(\frac{\partial\langle U_i\rangle}{\partial x_j} + \frac{\partial\langle U_j\rangle}{\partial x_i}\Big) - \rho\langle u_i u_j\rangle\Big\} \tag{2.7}$$

Here one note the addition of the term $\rho\langle u_i u_j\rangle$ which does not exist in the original Navier-Stokes equation and is denoted Reynolds stresses. The term leads to a closure problem as another term have been added, without any addition of another equation, and must be modelled in order to close equation 2.7 and it is this modelled term that leads to the different RANS models such as $k-\epsilon$ and $k-\omega$.

For this thesis, $Realisable - k - \epsilon$ and $k - \omega SST$ models were used, and will thus be the ones explained, they will however be denoted RKE and $k-\omega$ in the rest of the thesis if its not important to differentiate between $k-\omega$ and the SST addition. The stark difference between RKE and $k-\epsilon$ is that it adds a correction for cases where the normal stresses become negative for flows with sizeable mean strain rates [4]. This means that the standard $k-\epsilon$ can fail to predict flows involving rotation and separation, which is very prevalent for bluff body aerodynamics. RKE is written in equation 2.8 where one observes that the right hand is the Reynolds stress tensor that close equation 2.7.

$$\langle u_i u_j\rangle = \sum_i \langle u_i^2\rangle = \frac{2}{3}k - 2\nu_T\frac{\partial U_i}{\partial x_j} \tag{2.8}$$

Moreover, the first closure coefficient C_μ is a local function of the flow in RKE so that the negative term in equation 2.8 never can become larger than the positive term, which is important as the left-hand term is a sum of squares and can not be negative[4]. Another interesting feature of the RKE model is that realizability means that the stress tensor $\langle u_i^2\rangle\langle u_j^2\rangle - \langle u_i^2 u_i u_j^2\rangle \geq 0$[4] which if one recalls is the Schwarz's inequality which is an important feature in that it solves better for rotation and separation. [4]

The $k-\omega-SST$ uses $k-\epsilon$ in the free stream and $k-\omega$ to solve the wall bounded areas, thus $k-\omega$ will here be explained as $k-\epsilon$ have already been introduced. ω is defined as the specific dissipation, whereas ϵ is defined as the dissipation rate. The advantage of the $k-\omega$ model is that in low turbulent regions, $k-\epsilon$ must reduce at a correct rate which is hard to model [4]. No such problems occur for the $k-\omega$ model, furthermore it has been shown that it performs better in near-wall flows, and with a y+ low enough, no wall functions are needed. Lastly, it performs better in all boundary layers with adverse pressure gradients [6] which is an important feature and could be the difference why RKE failed in some cases, shown in the results of this thesis.

2.3 Numerical stability when modelling road vehicles.

At the beginning of the thesis, it should be noted that only RKE was decided to be used as turbulence model as it is a very stable and robust model. Furthermore, it was said that one of the convergence criterion to use was that C_d should vary less than one drag count for the last 1000 iterations, something that only RKE can achieve when applied to this type of CFD application [7]. However, it was found that for the tall IXTAboxes [190-60,170-60,150-60], RKE failed to model them correctly, most likely due to the shortcomings to model adverse pressure gradients, which gave a solution that almost looked like a compressor surge, which of course is entirely unreasonable. Thus $k-\omega$ was also used to get reasonable solutions to the tall boxes and verify it to RKE solutions. A drawback of $k-\omega$ is that it does not fulfil the original criterion stated, e.g. drag counts should vary below one count, and all residuals should be below $4 \cdot 10^-4$. Prior studies have also found that the value of ω at the inlet is sensitive to produce different solutions [7]. Since turbulent parameters are hard to estimate at the inlet, it was decided that $K - \omega$ with the SST addition was a better choice.

2.4 Sources of Drag

The primary sources of drag can be categorised as pressure drag and friction drag, both are related to losses in total pressure, which in combination with the pressure increase at the stagnation point located at the front of a car leads to a ∇P between the front and back of the car. This pressure difference gives rise to suction from a force perspective gives rise to drag force whose vector is in the negative driving direction. The total drag can be written as in equation 2.9 where C_d is the sum of all drag contributions specified below.

$$\frac{F_d}{A_p} = C_d \rho U_\infty^2 \tag{2.9}$$

2.4.1 Friction Drag

Frictional drag accounts for roughly 10-12% of the total drag[8] when it comes to external flow over vehicles. The source of friction drag stems from small crevices and other irregularities on the surface, giving rise to friction losses [1]. The air that is flowing over the object will as a result lose its total pressure to useless heat and is evaluated as seen in equation 2.10

$$\frac{F_d}{A_s} = C_f \rho v_\infty^2 \tag{2.10}$$

The local skin friction coefficent is calculated locally as seen in equation 2.11.

$$C_{fx} = \frac{0.664}{\sqrt{Re_x}} \tag{2.11}$$

This value can be integrated to a mean skin friction used in equation 2.10 through equation 2.12

$$C_f = \frac{1}{A_s} \int_{A_s} C_{fx} dA_s \tag{2.12}$$

In CFD applications, C_{fx} is calculated to a discrete value for each surface cell element which means that equation 2.12 is summed instead of integrated. It should also be stated that evaluation of the skin friction in CFD applications is an effective way to improve the design as one can see where flow separation has occurred which is a source of wake drag [9]

2.4.2 Drag due to flow separation

As the projected area of the car changes in the X direction, so will the pressure over the car change, as static pressure is converted to dynamic pressure as the area increase and converted back again as the area decreases. This means that on the interval $[A, A_p]$, the pressure flows against a positive static pressure gradient, while on the interval $[A_p, A]$, the flow is flowing against an adverse pressure gradient. If one recall the theory in section 2.1.1 this could give rise to flow separation, which induces drag. In vehicle applications, this often happens on the back window if the angle between the window and the horizontal line is too large, and can be observed using a scalar plot of the skin friction as the skin friction have a much lower value on surfaces where flow separation have occurred, compared to the mean value of skin friction.

2.4.3 Wake Drag

A particular case of drag due to flow separation is the wake drag, the wake drag is formed when the flow passes over the car's back, and the angle is steep enough to cause flow separation. The shear stress on the flow causes it to deviate from the *would be* inviscid streamlines. This deviation from the inviscid case is seen as flow separation which produces eddies of various sizes, thus instead of ideal total pressure recovery in the wake, which would be achieved in an inviscid case. Some of the energy in the flow is spent in the production of turbulence. For the case of turbulent kinetic energy, when kinetic energy is spent on sustaining the eddies, the only way of energy conversion is through the energy cascade where large eddies break to form smaller eddies, which eventually dissipate into heat[4], making it is a loss of total pressure recovery.

3 Literature Study

The role of the literature study is to map prior work and emphasise engineering rather than physics that was done on the theory chapter

3.1 Aerodynamic devices

A large part of this thesis has been developing improvements to the IXTAbox to reduce its drag. Thus, a literature survey into prior work regarding aerodynamic devices has been done to inspire this thesis. It should also be noted that aerodynamic devices commonly used on both trucks and passenger cars have been implemented as one could look on the IXTAbox as a miniature cargo trailer.

3.1.1 Passenger Cars

A myriad of aerodynamic devices exists today, some to create downforce, some to reduce noise and some to reduce the drag. When it comes to drag-reducing devices, diffusor extenders and baffles were found especially interesting to apply to the IXTAbox. When it comes to the IXTAbox, one could look at it as one natural diffuser extender if the gap between the box and car could be removed. One could also look at the geometry of the floor plate on the box and improve its design with the aid of baffles or its geometry. The paper *A Study of an Active Rear Diffuser Device for Aerodynamic Drag Reduction of Automobiles* looked at various designs for diffusor extenders, where they found the geometry of the arc plate to reduce the drag by 20 counts and the square diffusor plate by 18 counts[10]. However one could question their convergence criterion as they are weak, they state a running time of +10h and continuity residual below 10^-4 to be their criterion while no mention of force monitors was stated. However, they use RKE, a stable and robust model which should converge after +10h, and the results are interesting enough to bring up in this study.

The thesis *Aerodynamics Concept Study of Electric Vehicles Drag Reduction and Range Increase* studied amongst other things baffles on the underbody of the DrivAer to some success, a drag reduction of 5 counts was achieved [11]. Moreover they studied diffusor extender which gave the idea that the IXTAbox could with modifications act as a diffuser extender.

3.1.2 Trucks

As mentioned earlier, one could look at the the gap that forms between car the the IXTAbox as an analogy to the gap that is formed between a truck and its trailer to which many aerodynamic studies have been done. With that in mind, there are several aerodynamic devices unique to trucks, they include but are not limited to:

- Tear drop shaped trailer
- Sealed Gap between truck and trailer
- Vortex Stabilisers
- Side Plates

The tear drop shaped trailer changes the shape of the roof on the trailer, from flat to curved with the goal to improve the flow over the roof, which reduce the base wake volume. The sealed gap between truck and trailer adds plates to cover the trailer face, facing the the driving direction so that no stagnation can occur on the surface. If a sealed gap is not possible one can also add a vortex stabilizer, which is several plates that run along the vertical axis to divide the flow into several sections so that no air can move in the j direction between two different sections. The side plates are put on the back of the trailer, and move the flow separation further away from the back of the trailer for the flow coming from the sides. All these improvements have been used an inspiration for this thesis

3.2 Roof boxes

As mentioned in the introduction, roof boxes is not something that has been studied in the same way as cars have, for one the roof box industry does not have the same means as a car company have to perform aerodynamic studies. Car companies have no desire to perform tests for auxiliary equipment, and fuel prices have historically been low. Nevertheless, some studies exist and will be discussed.

Putting any object on the roof of the car is a very sensitive parameter, when racks are added, a 9% increase of C_d has been noted, putting a roof box on the same rack increase C_d by 24%, and increases of 30% is not unheard of[8]. Furthermore, the frontal area increases, which increases the total drag force even more. Something that is important to carry in mind, but that is not studied in this thesis is that a roof box changes the driving performance, as the center of gravity is affected, something that affect the moment forces acting on the car. Furthermore, the wake produced by the roof box is acting much higher Z coordinates than the wake of the vehicle. This will, of course, affect the direction of the drag force vector and could shift the wheel load from the forward wheels to the back wheels. Finally, when exposed to side winds, the rolling moment is acting on surfaces at a higher position which by observing equation 3.1 makes it obvious that the roll moment increase by just having the extra length away from the centre of mass. [8]

$$M = l \cdot F \tag{3.1}$$

Furthermore, it has been shown that the position of the roof box is a sensitive parameter to both C_d and C_l where *Examining influence of a rooftop cargo carrier position on automobile aerodynamics* found that the drag change compared to a base case of DrivAer estateback + roof box similar to what is denoted as *Roof Box Cargo* in this thesis, could be almost 30%. The primary reason was found to be that the interference drag between car wake and box wake can almost be removed if placed correctly, the essential parameter was the airflow between car roof and box bottom, which, if designed correctly, could shield the two wakes from each other[12]. This is not something that has been studied in this thesis regarding the two roof boxes due to time constraints. Thus one should take the values with a pinch of salt, however, the results found in this thesis fall into the same range as presented in *Aerodynamics of Road Vehicles*[8] and are deemed reasonable, and gives good insight to which phenomena that increase drag the most, and the differences between a roof box, and an IXTAbox.

4 Method

As CFD analysis around roof boxes are rare and tow bar mounted boxes non-existent, the method chapter will aim to as thoroughly as possible explain the numerical setup so that validation or further studies by another engineer is possible by reading the thesis.

4.1 Test Object

As mentioned in the introduction, the test object used in this study is the DrivAer Notchback model, and the following simplifications have been done to the geometry.

- Smooth under body
- Closed rims
- Removed Mirrors
- Removed handlebars on doors

These simplifications to the geometry is visualised in figure 4.1.

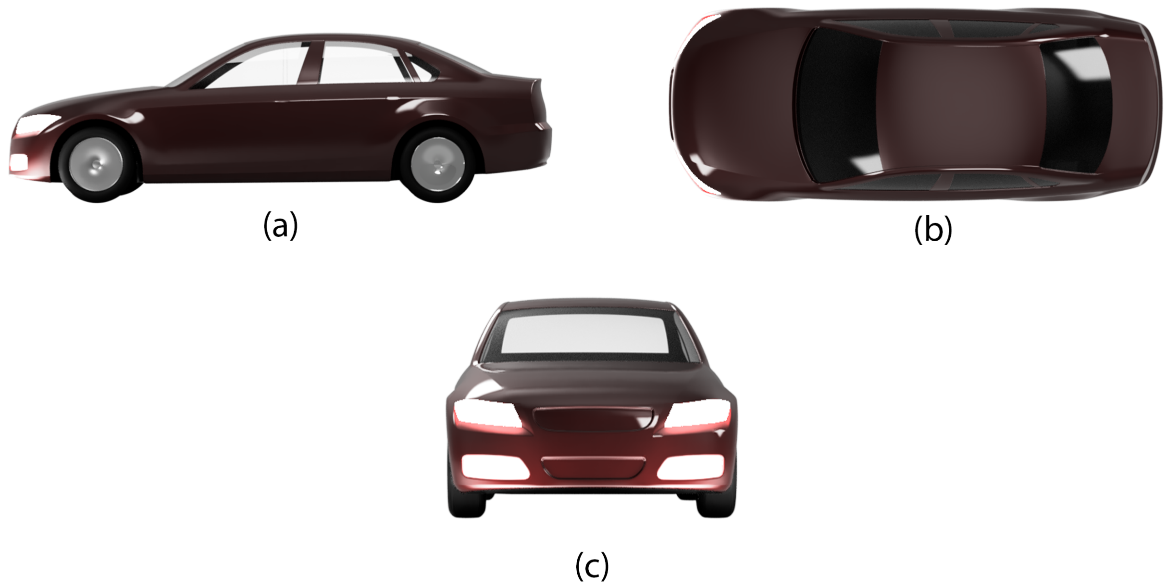

Figure 4.1: *Overview of the DrivAer model with stated simplifications done to the geometry. (a) shows the model from the side, (b) from the top and (c) from the front.*

The modifications have been done to simplify the geometry, without removing the complexity of the relationship between cargo box and car. Thus reducing computational cost without compromising quality. For example, the handlebars would require a very fine surface and volume mesh, but its influence on the downstream results are deemed to be very small, making it a reasonable simplification. To do the modifications to the CAD file received, the work was carried out in the pre-processor *Ansa*. The smooth underbody and closed rims were already a possible choice in the CAD file received and did not need any further modifications. Finally the model was made watertight to not pose a problem when meshing the surface, for that the geometry was cut in half along the symmetry plane of the car to decrease the workload by half. As a last measure before export to *Star CCM+* the CAD drawing was copied, mirrored and stitched together again to create perfect symmetry. In figure 4.2 one can see the final *CAD* model with both the roof box named *Streamlined* and an IXTAbox *170-40* to visualize where they are placed when implementing it to *Star CCM+*.

Figure 4.2: *Cad drawings of the cargo boxes and their position relative to DrivAer, (a) is with the streamlined roof box, (b) is the 170-40 IXTAbox*

4.2 CAD drawings of IXTAbox and roof box

As no cad files exist for roof boxes, the cad files for IXTAbox were done in AutoDesk "sheet metal" cad tools which the surface wrapper handled poorly. It was decided to use Fusion 360 to create proper cad files for CFD, as they were properly prepared in CAD, no *Ansa* work was required and could be imported directly into STAR-CCM+.

Six different IXTAboxes have been modelled. They vary in height and width, while the depth is constant. The sizes come in the following order: $[190-60, 190-40, 170-60, 170-40, 150-60, 150-40]$cm where the first number indicates the length, and the second number indicate height. When it comes to IXTAbox, it would be possible to pre-process the files in *Ansa* to close the geometry, as there are gaps between the sheets of metal that are not of interest to this CFD study. It was then realised that since there are many symmetries in the various IXTAbox models, the difference between 190-60 and 190-40 model was only the height of the lower part of box. Thus a simple extrusion of the bottom face on 190-40 would produce a 190-60 box, similarly, by cutting the box in half and removing 20 cm, one could take the 190-60 box and convert it to a 170-60 box in one simple CAD operation.

Thus time was spent to produce a solid geometry of the IXTAbox, and then do these simple operations to produce a box that does not require any ANSA work at all, it could directly be imported into *Star CCM+*. In figure 4.3 one can see how the $190 - 40$ and $190 - 60$ box looks like when importing them to *Star CCM+*.

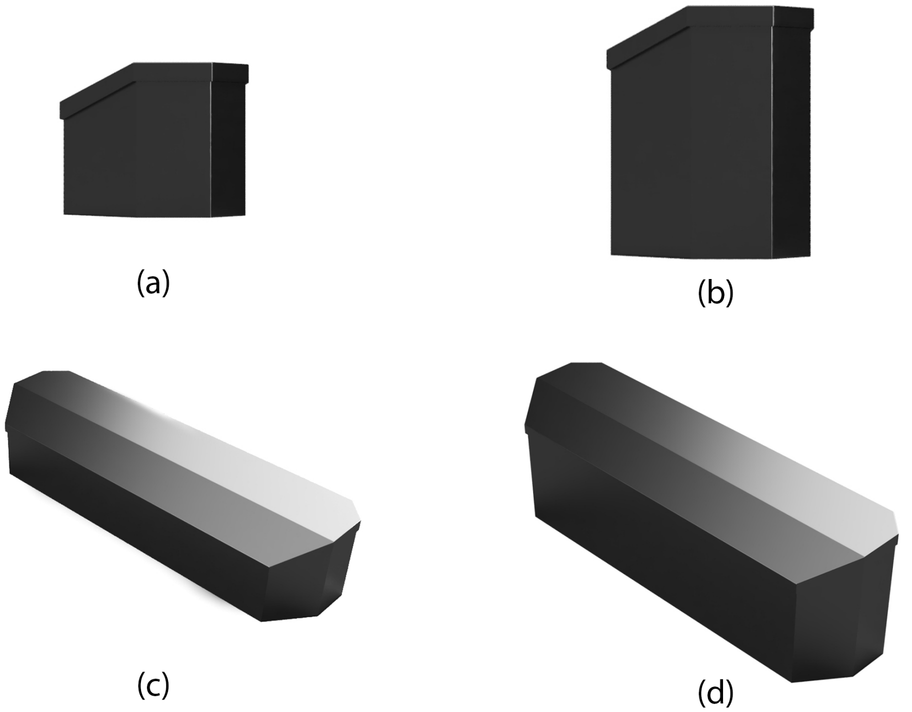

Figure 4.3: *Cad drawings of the 190 box with 40 and 60 cm height variants. (a) is the 190-40 from the side, (b) is the 190-60 from the side, (c) is the 190-40 from above and (d) is the 190-60 from above. When it comes to the other boxes, they have the exact same measurements, except for a width reduction.*

In the case of the roof boxes, two existing roof boxes were used as inspiration, one streamlined and one large, where volume is emphasised. 2-D images of the roof boxes were imported into Fusion 360 to be used as a background canvas from the side and above. The volume box has approximately the same volume as $[190 - 60, 190 - 40, 170 - 60]$ while the streamlined box has approximately the same volume as $[170 - 40, 150 - 60, 150 - 40]$. As the manufacturer provides the total length of the roof box, one could calibrate the 2-D image so that the length inside the CAD program corresponds to the actual value, then a cuboid was created to where length, height and width correspond to the maximal values of the box. Using the 2-D pictures, cutaways on the cuboid was done to get the final shape, the resulting roof boxes can be observed in figure 4.4

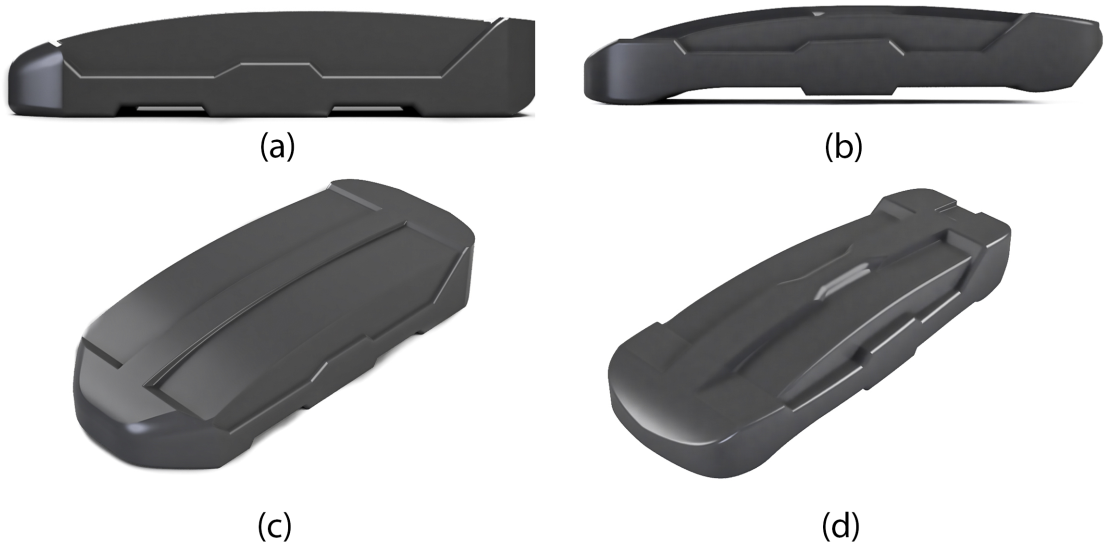

Figure 4.4: *Cad drawings of the two roof boxes drawn for the thesis. (a) is the so called volume box from the side, (b) is the so called streamlined box from the side, (c) is the volume box in 3-D, (d) is the streamlined box in 3-D.*

4.3 Computational domain and numerical setup

With the test objects created and cleaned, they are imported to *Star CCM+* to a simplified wind tunnel as observed in figure 4.5. To combat problems arising from the boundary conditions, such as back flow at the outlet, are solved by large distances between boundaries and test object. Furthermore the distance between test object and inlet in smaller than test object and outlet, so that one can analyze the wake developments far away from the car if necessary.

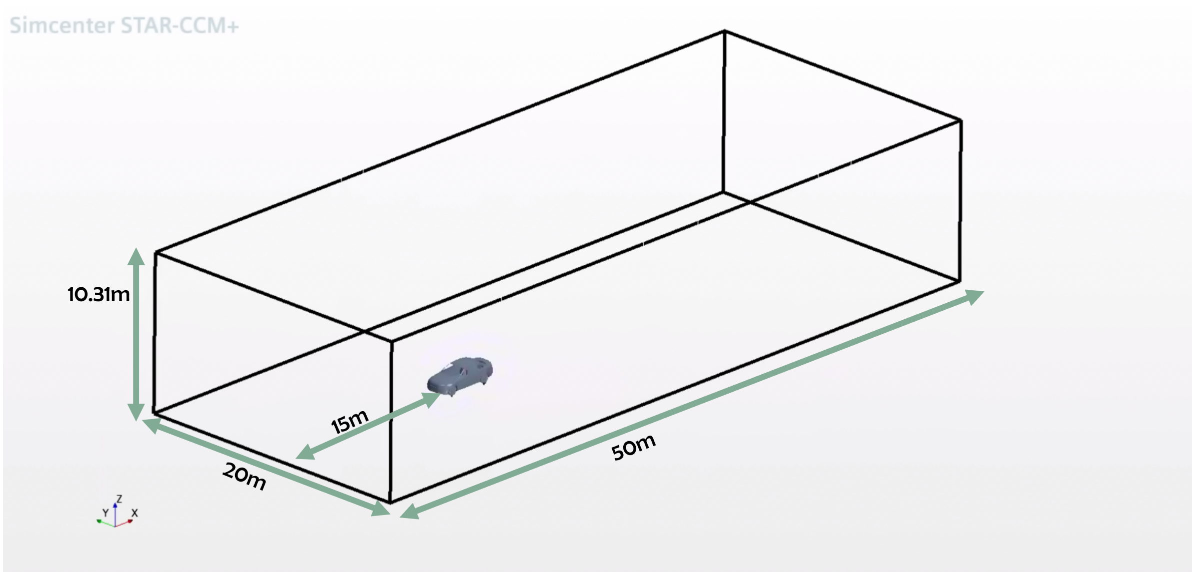

Figure 4.5: *Overview of the test object's placement inside the simplified wind tunnel*

The inlet condition was decided based on what should be normal conditions, e.g. a car travelling with a roof box or IXTAbox is likely on the road to a ski resort, e.g. roads where around 90 km/h are conventional. Since the car is stationary in *CFD*, and the fluid moves over the car the fluid will build a boundary layer on the ground, which is not a natural phenomena in this application since it is the car that moves in a real case. Thus the ground was set to moving ground so that the speed of the fluid and ground is the same – e.g. no boundary layer is built. Similarly, the wheels are by default stationery in *CFD*, however numerous studies have shown that Cd decrease with rotating wheels rather than stationary, furthermore it is in the same range of Z-planes where the IXTAbox is located, meaning that upstream flow conditions are essential to model as natural as possible since it is very likely that it will affect the flow downstream where the IXTAbox is located. Thus four local coordinate systems are created, with origin in the centre of each rim, then the vectors for the local coordinate system is set to unit vectors, here the author would like to stress that it is vital to set them precisely to unit vectors as they will produce significant errors for minor user errors, such as using the graphical tool to create the local coordinate systems. The angular velocity is calculated to 78.5 Rad/s if the outermost point on the wheel is to spin at 25 m/s as it should. In table 4.1 an overview over the boundary conditions can be seen.

Table 4.1: Overview of important settings to the boundaries

Boundary	**Type**	**Value**
Inlet	Velocity Inlet	25 m/s
Ground	Moving Ground	25 m/s
Windtunnel Sides	Symmetry	-
Wheels	Rotating Reference Frame	78.5 Rad/s
DrivAer	Wall	-
Boxes	Wall	-
Outlet	Pressure outlet	0 Pa

The Sides of the wind tunnel is compromised by three faces, left, right and top and are set to symmetry planes. DrivAer and corresponding boxes are of course set to wall and no slip as they are solid objects. Finally the outlet is set to a conventional pressure outlet at 0 gauge pressure.

4.4 Mesh generation

The DrivAer model has been extensively studied in the previous thesis and research work, where a mesh size lies between $20 - 50 \cdot 10^6$ cells depending on what the purpose of the study is[13],[11],[14]. A mesh dependency study also shows that after around 40 million cells, the mesh dependency of C_d converges to a fixed value. With this in mind, it was decided that around $30 * 10^6$ cells would be a target that compromise between accuracy and CPU hours, the outcome of the goal is shown in table 4.3. The goal was allowed to be breached for the two roof boxes, and some of the improvements done on the box to satisfy best practice of meshing.

4.4.1 Surface Mesh

As the imported DrivAer contained many cad errors that would lead to divergence, a surface wrapper in combination with surface remesher was used. For the surface remesher, the minimum surface quality of 0.2 was selected, which is the highest setting allowed, it led to longer meshing times since more meshing iterations ran, but as the mesh quality improved, it was well-spent processing power. When it comes to the mesh size on the surface, the wheels were allowed to go down to 20% of the original base size as seen in table 4.2. This is because the wheels have continuous curvature, thus requiring smaller mesh to stay as close as possible to the cad file as possible.

Table 4.2: Surface mesh size as function of mesh base size

Surface Mesh	Minimum Size	Target Size
Wheels	20%	100%
Car	30%	100%
IXTAbox	13.3-30%	100%
Roof boxes	30%	100%

It should also be noted that some of the improvements done on the IXTAbox does not follow the exact order stated in table 4.2 As they have very fine details that was not captured with 30% minimum target size, the target size was the same however.

4.4.2 Prism Layers and Y+

Regarding prism layers & y+, since the choice of turbulence model fell on RKE, a y+ value in the range of 30-200 have been recommended as best practice[15], a value below or above the stated range could give rise to loss of accuracy. The same prism settings were also used for $k - \omega$ so that as many settings are kept equal as possible.

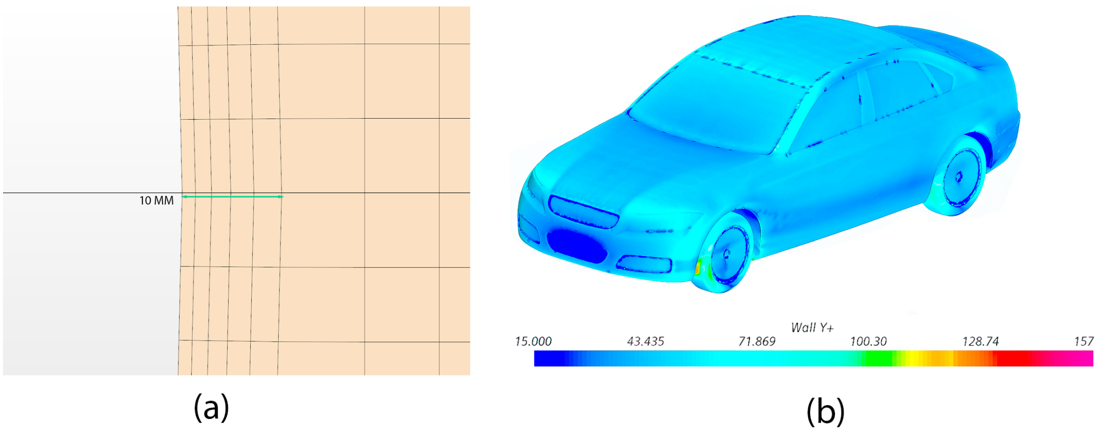

Figure 4.6: *Image (a) shows the prism layers and their length, from the figure one can see that the total layer is 10 mm, and that 5 prisms are used. Image (b) shows the corresponding y+ on the surface of DrivAer, most of the car have a y+ of roughly 60 while some areas such as the stagnation point in the grill have a lower value than 30.*

As the geometry is quite complex, there are no analytical solutions to finding the y+ for these types of boundary layers with complex curvature, stagnation points and flow separation. However, an estimate was made based on flat-plate boundary layers theory. With five prism layers and a growth factor of 1.2, it gave the first estimate of y+, which was implemented in the mesh settings, then the solution was allowed to run 500 iterations and evaluated. It was observed through Star CCM's y+ scalar function that the value was a bit too low, with this estimate forming a foundation, an iterative approach was made to find a more optimal value, it required two iterations before settling on a total height of 10 mm, 1,2 growth layer and five prism layers. The results can be seen in figure 4.6. It is noted, however that some areas with stagnation have y+ values below 30, however they are rare, and it was advised to not spend too much time on separating surfaces parts and do individual y+ settings for each surface part, such as the grill[15]. For future work, one could try to use different y+ settings for different parts and make the last layer a little bit bigger so that it is half the cell size of the first normal cell, as it is now one third as seen in figure 4.6

4.4.3 Volume Mesh

The volume mesh use the trimmer geometry as the domain is very large, thus one can optimise the number of cells when using the trimmer compared to other mesh geometries. The growth and size of the volumetric refinements can be seen in table 4.3.

Table 4.3: The volumetric refinements can be seen below as a percentage of the base size equaling 15 mm

Volumetric Refinement	**Size**
Wheel	10%
Wake XS	50%
Wake S	100%
Wake M	300%
Wake L	600%
Wake XL	1200%

Here, care have been taken so that the cell growth is done in an orderly fashion, either increasing by a multiple of two or three, which is important to counteract numerical diffusion. In figure 4.3 one can observe from a top and side perspective the growth of the mesh. One can see the most refined mesh size from the side, eg 50% of the base size. Furthermore, the Wake XS refinement was also allowed to extend up to the back window, as flow separation is likely to occur in that area due to adverse pressure increase.

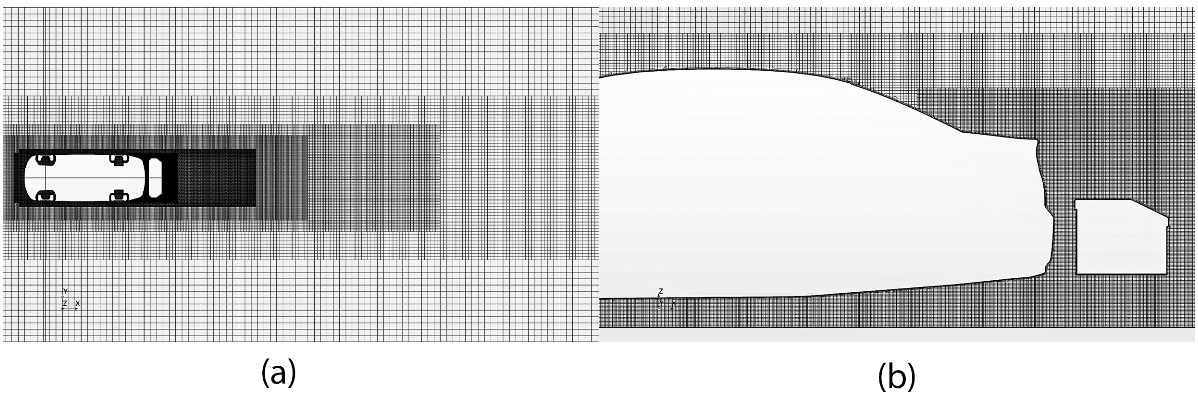

Figure 4.7: *(a) Volumetric refinement overview in the Z-plane where incremental increase of mesh size is displayed (b) Symmetry X-plane where one can see Wake XS, Wake S and Wake M in increasing order*

4.5 Convergence criterion

The convergence criterions are judged by:

- All residuals below 10^-4 (10^-3 for $k - \omega$)
- C_d is varying below 1 count for the last 1000 iterations (2 counts for $k - \omega$)
- The solution looks reasonable, eg expected flow directions, velocities and symmetrical where symmetry should exist for a steady state model, such as left and right side of the car.

When the convergence criterion where decided, the plan was only to run $Rk - \epsilon$, which have been proved before to be the only model that fulfils the criterion of count variation below 1[7]. However, the criterion was required to be relaxed to accept the results from the studies using $k - \omega$. They were allowed, as they followed a reasonable trend, reasonable solution and the count variation was still at two counts.

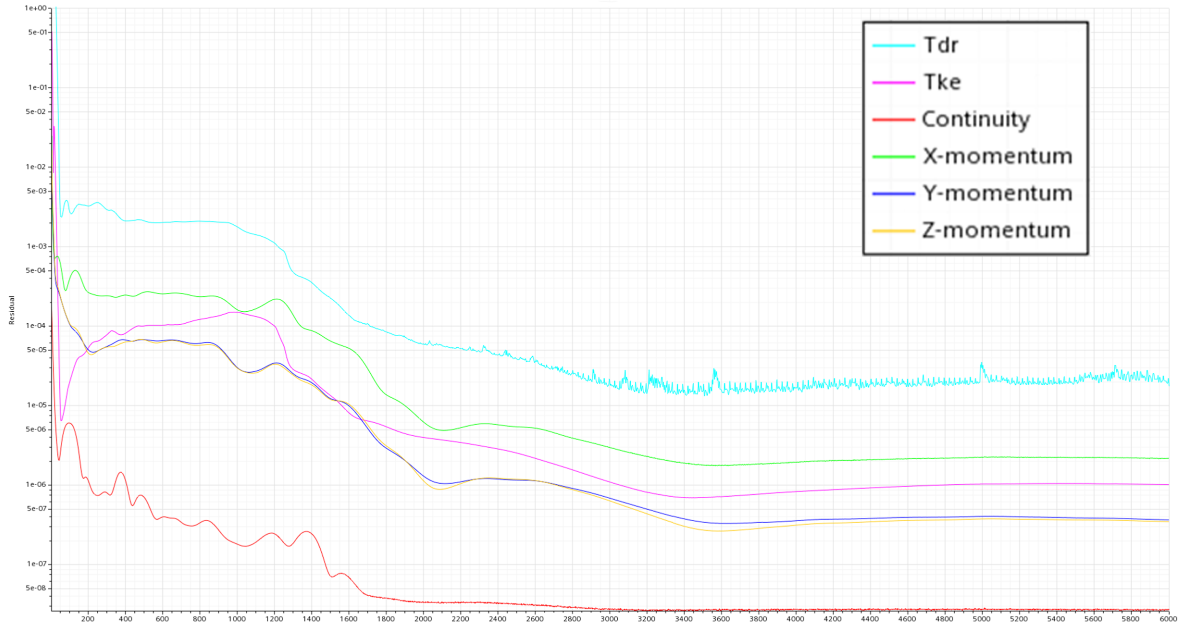

(a)

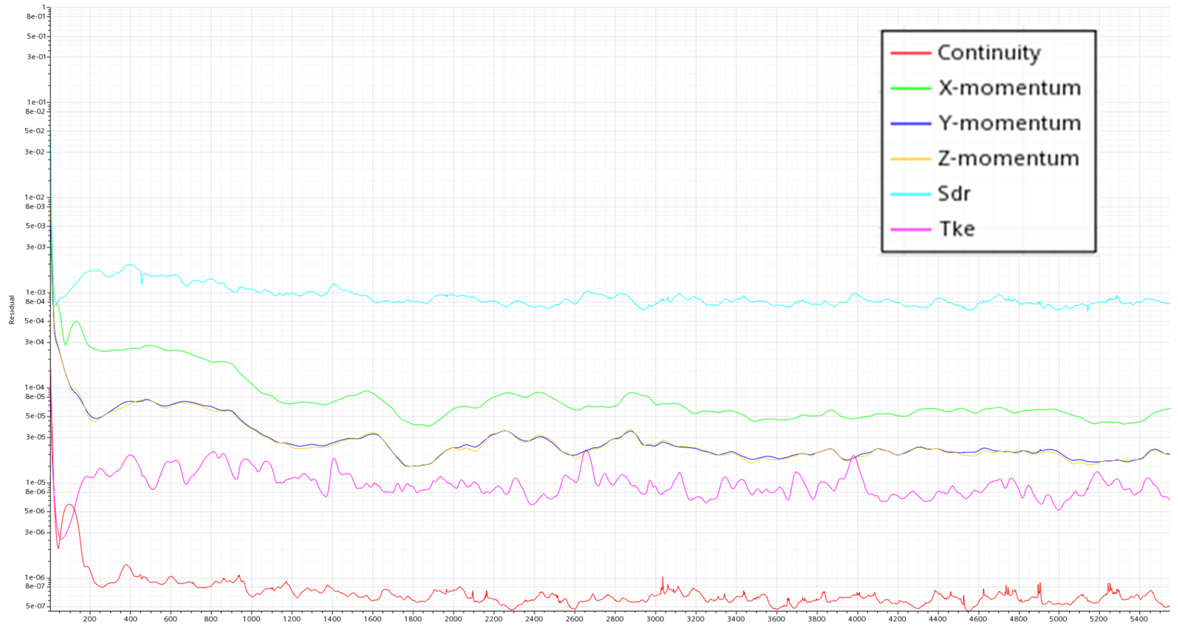

(b)

Figure 4.8: *(a) Residual overview when using RKE. (b) Residual overview when using $k-\omega$. Here one observe for example the robustness of the $Rk-\epsilon$ as periodic oscellations are almost non existant whereas $k-\omega$ have oscillations, this translates also to the C_d monitor. Note that the colours for (a) and (b) change meaning as seen in the legend.*

5 Results

The results chapter has the following structure: first, a little amuse-bouche is presented in the form of a table consisting of C_d, area and C_dA values for the base case, two roof boxes and six IXTAboxes for both turbulence models. Then the base case of a DrivAer notchback is presented, the wake structure is discussed but will extensively be compared to the wake when introducing roof boxes and IXTAboxes. Lastly 10 improvements to the IXTAboxes shall be done to map sensitive areas of the IXTAboxes, to show what part of flow modifiers have an actual affect on the car.

Table 5.1: C_d, the total projected area, and corresponding C_dA using DrivAer, roof boxes and all IXTAboxes using both turbulence models

Model	$C_d\ k-\omega$	$C_d\ RKE$	**Area** (m^2)	$C_dA\ k-\omega$	$C_dA\ RKE$
DrivAer Alone	0.254	0.257	2.106	0.536	0.541
Streamlined roof box	0.307	0.303	2.407	0.740	0.730
Volume roof Box	0.310	0.312	2.472	0.769	0.771
150-40 IXTAbox	0.263	0.259	2.106	0.554	0.545
150-60 IXTAbox	0.281	0.278	2.106	0.592	0.586
170-40 IXTAbox	0.263	0.264	2.106	0.555	0.557
170-60 IXTAbox	0.281	0.307	2.108	0.596	0.647
190-40 IXTAbox	0.282	0.275	2.152	0.603	0.592
190-60 IXTAbox	0.283	0.322	2.183	0.618	0.678

Some remarks to table 5.1 should be done before showing each case, it was expected that the two turbulence models would show slightly different values compared to each other. However care should be taken regarding the IXTAboxes of height 60 using RKE as it will be shown later how it fails. Furthermore, it is only the [170-60,190-40,190-60] boxes that increase the area, while the other IXTAboxes are entirely covered by the car. Moving on, it is noted that C_d when using $k-\omega$ is both higher and lower than RKE. This means that no constant trend is obtained such as $k-\omega$ is always 2 counts higher than RKE. The only reason why $k-\omega$ is also used is due to the fact that RKE failed to model the IXTAboxes of height 60. Thus a comparison study was required, where $k-\omega$ could be compared to known C_d values using RKE so that the C_d values of the IXTAboxes of height 60 could be accepted, as they have no comparative turbulence model to validate their numbers. By observing the reported numbers in 5.1 it is seen that $k-\omega$ is less stable, as was verified by residuals and force monitors, but it predict the flow in a more reasonable way for boxes of height 60.

5.1 Reference: Drivaer notchback

As no literature exists for a tow bar mounted box and very little for roof boxes, it was deemed a base case where one can compare the quality of the CFD setup to that of others was necessary. Luckily, there is abundant amount literature on DrivAer, which is the car model used.

Comparing the two turbulence models in a qualitative manner, one can see in figure 5.1 that the two turbulence models predict the same base pressure on all surfaces that is not in the wake of the car. The wake on the other hand is much more complex, where the models start to differ in the base pressure that they model, however on average the base pressure must be similar since C_d is very similar for both cases. But it can be seen using RKE that an almost perfect pressure recovery is achieved around the middle section of the car, while the simulation predicts an unclean flow separation on the sides of the trunk. Moving on to $k-\omega$ in figure 5.1 it is seen that the pressure recovery is more evenly distributed across the trunk of the car. On the other hand, the recovery itself is slightly negative compared to the almost perfect pressure recovery in the middle section using RKE. Finally it is seen that $k-\omega$ predicts cleaner flow separation around the trunk, and that the pressure around the wheels are higher.

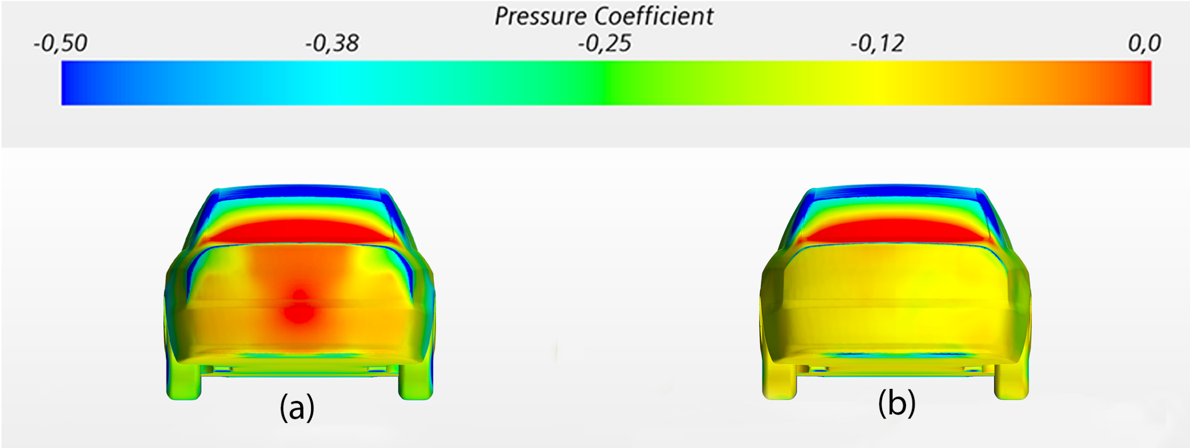

Figure 5.1: C_p *from behind comparing the pressure acting the cars surface for the turbulence models, (a) is when using* RKE*, (b) is when using* $k - \omega$

In figure 5.2 one can see the velocity streamlines and their interactions in the wake, the flow coming from the sides, go to different parts of the wake, as flow coming from the c-pillar region using $k - \omega$ goes to the sides while for RKE it goes to the middle. Comparing the streamlines to the pressure recovery, it is seen why the pressure recovery is stronger for RKE in the middle section, as the magnitude of the streamlines is much lower.

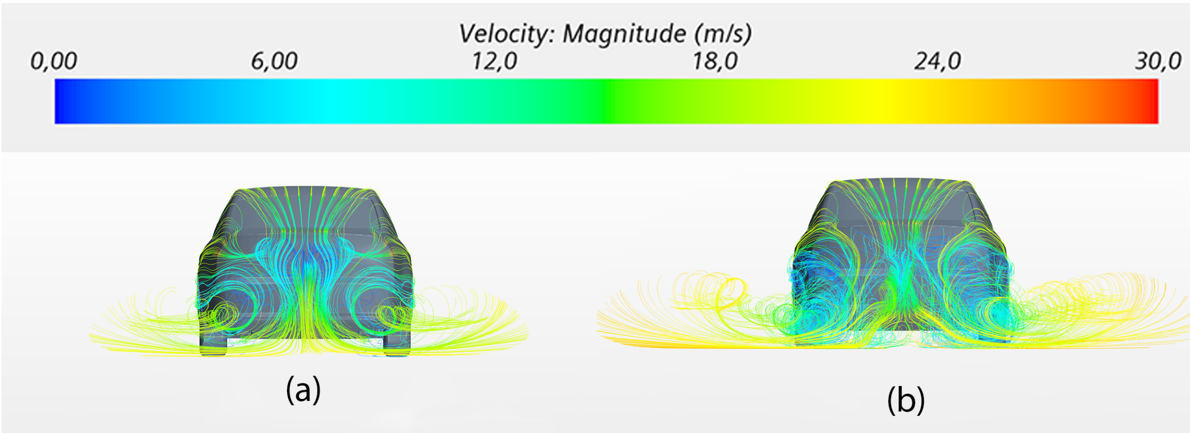

Figure 5.2: *Streamlines coming from the sides, top and under-body of DrivAer, mixing to form a dead wake.(a) is when using* RKE*, (b) is using* $k - \omega$*.*

Furthermore, both solutions are deemed symmetrical by studying the two halves of the symmetry plane that run in the X-Z plane and where Y is zero. This is important, as one of the convergence criterion was to have a symmetrical solution where symmetry should exist, when qualitatively studying the images produced in post-processing. However, because the residuals are periodic even when converged using $k - \omega$, it does carry some asymmetrical details. These details are easy to spot in figure 5.3(b), C_{ptot} in a wake plane $0.1m$ away from the car is shown where for example, the right-hand side and left-hand side, just above the wheels, are somewhat different, which was also seen in figure 5.1.

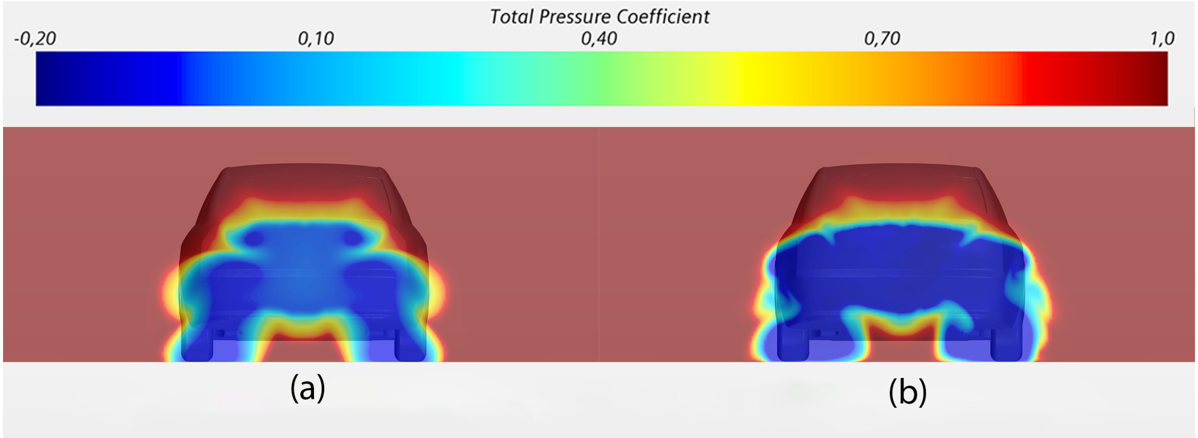

Figure 5.3: C_{ptot} *on wake plane 0.1m away from the car is shown, (a) is when using* RKE*, (b) is when using* $k - \omega$

5.2 Reference: Roof boxes

For the roof boxes, when looking at the velocity plots from the side, as in figure 5.4, one can directly see how roof boxes increase the wake volume, since there is another object on top of the car, more interestingly however is that fact that the two wake volumes blend, to impact each other in a negative manner creating even more turbulence in the wake. Analyzing the streamlined roof box in figure 5.4 one can see at the back of it, how it changes angle, to steer the flow, on the top of the roof box downwards. This aid the pressure recovery as a smaller wake volume is induced as well as the relationship between upwash and downwash is stabilised. The so called volume roof box does not have this feature, which induce a larger wake volume. Comparing the reference in figure 5.4 to the two roof boxes, we can thus conclude from the scalar plot that putting on a roof box does not impact the upwash in the wake behind the car which is said by comparing the reference and the volume roof box and their wake structures behind the diffusor of the car. However a roof box can influence the downwash if designed properly.

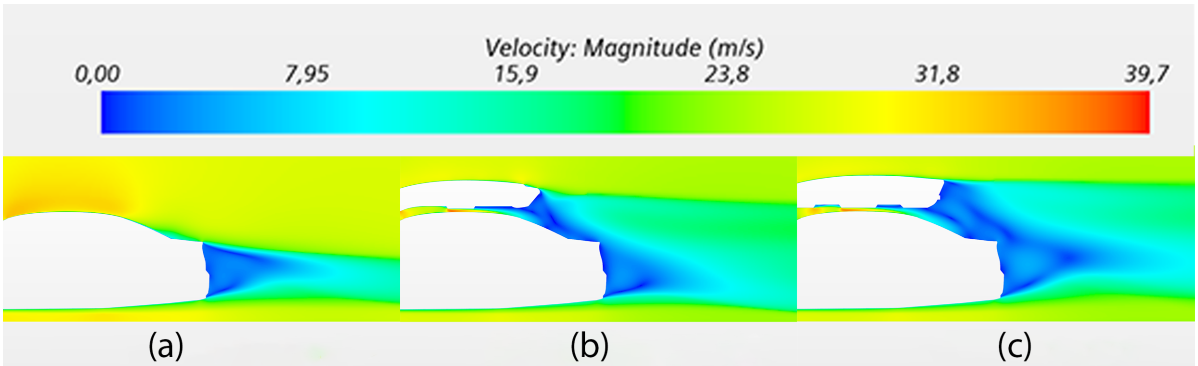

Figure 5.4: *Velocity magnitude in XZ-plane for Y=0 using* RKE*. (a) is the DrivAer for reference, (b) is the streamlined box (c) is the volume box. For example one can see how the design to create more downwash on the streamlined reduce the wake volume.*

Furthermore, the wake starts already at the back window due to the complex relationship between the adverse pressure gradient that occur for the flow going between roof and box and the wake that is formed behind the box. On the other hand, *DrivAer* have a small flow separation that reattaches itself on the top of the trunk as seen in figure 5.4. As the flow impact the back window when using a roof box, there is a strong correlation to the pressure recovery on the window section that needs to be investigated.

In figure 5.5 one can observe the pressure recovery on the surfaces from behind and should be compared to figure 5.1 using *RKE*. Compared to when only using the *DrivAer* model, it can be seen that the pressure recovery is strongly affected by the roof box, as predicted. Where for the reference there was a pressure recovery on the back window, it is essentially now removed using a roof box. The pressure recovery on the box itself can be said to be rather lacking, mainly due to the fact that the flow separates before reaching the sharp edges in the back, leading to an unclean flow separation.

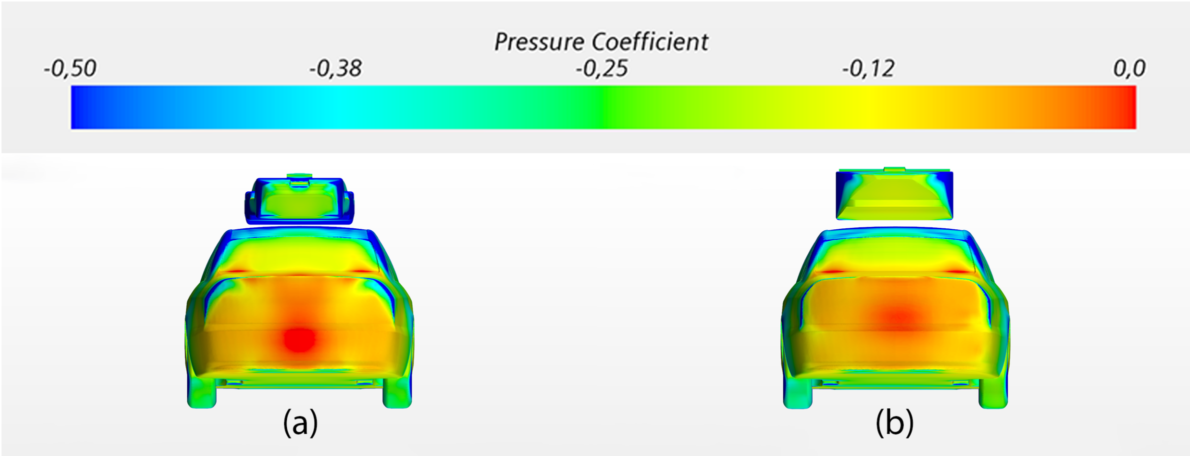

Figure 5.5: *C_p plots from behind for the two roof boxes using RKE, (a) is the streamlined box while (b) is the volume box*

When it comes to the pressure recovery on the trunk, where the wake behind the vehicle is normally found. It is seen that for the *streamlined* case, that the impact is rather low, despite the face that it increases the downwash. The flow separation on the sides of the trunk are similar compared to when only using *DrivAer* in figure 5.1 while the intense red dot in the middle section exists for both cases. The *volume* roof box on the other hand, predicts a cleaner separation behind the trunk and more evenly distributed pressure recovery.
When analyzing the total pressure by comparing the images in figure 5.6 to the reference in 5.3(a), one can see that the wake development further away from the car stands in stark difference between the two roof boxes, and to the reference. The *streamlined* roof box, as have been mentioned before increase the downwash strength, the impact on the total pressure is that the wake behind the trunk , get pressed to the as the force from above increases. On the other hand it still predicts the formation of the small vortices leaving the top the the trunk which is also observed on the reference case. The wake structure that comes from the back window is at 0.1m away from the car weak, as the most intense wake from the roof box follow the car, along the back window down to where the wake is normally located.

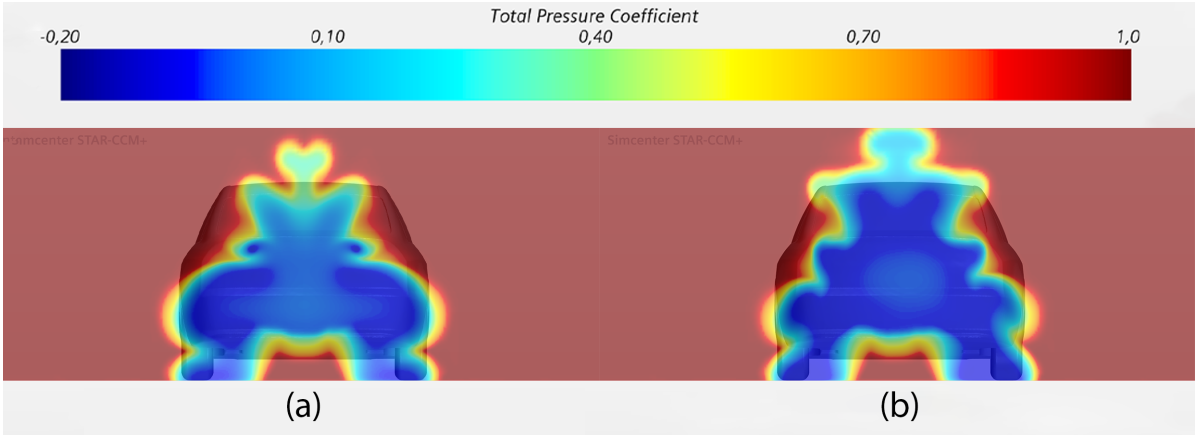

Figure 5.6: C_{ptot} *plots using RKE 0.1m away from the car and in the YZ-plane, (a) is for streamlined box (b) is for volume box*

When it comes to the *volume* box, it can be see that the wake structure is much larger. especially for the wake leaving the back window likely due to the fact that the model doesn't affect the downwash as much as the *streamlined* box does. This can be verified by the fact that there is no indication that any meaningful amount of force is done on the wake leaving the trunk, as the *volume* box and the reference in figure 5.3 appear similar. Finally it appears that the pressure recovery from the flow that goes between the box, and roof of the car is much more effective on the *streamlined* version than the *volume* version by observation of total pressure combined with pressure on the surfaces.

5.3 Reference: IXTAboxes

Six IXTAboxes have been studied, and will be presented in this chapter. First of all, the 170-40 box will be used as comparison for the other boxes, comparing RKE solution to $k-\omega$ and showed from different angles. Then the 60 boxes that were only modelled with $k-\omega$ will be discussed and compared with the 170-40 box using $k-\omega$ while the 190-40 and 150-40 boxes will be compared to the 170-40 box using RKE

5.3.1 170-40 using RKE and $k-\omega$

The fact that the increase of C_d is low for the IXTAbox compared to a roof box, is of course good news, however it will be seen in this section how the wake structure changes rather drastically with the IXTAbox. When it comes to the pressure acting the on car and box, as seen in figure 5.7 the pressure recovery on the car itself has increased compared to the reference *DrivAer*. This stands in stark contrast to the roof boxes which decrease the pressure recovery both on the back window as well as the trunk. However, the box surface facing the car, is a new surface to which stagnation is observed while losses are created in the wake following the box which lead to a non ideal pressure recovery.

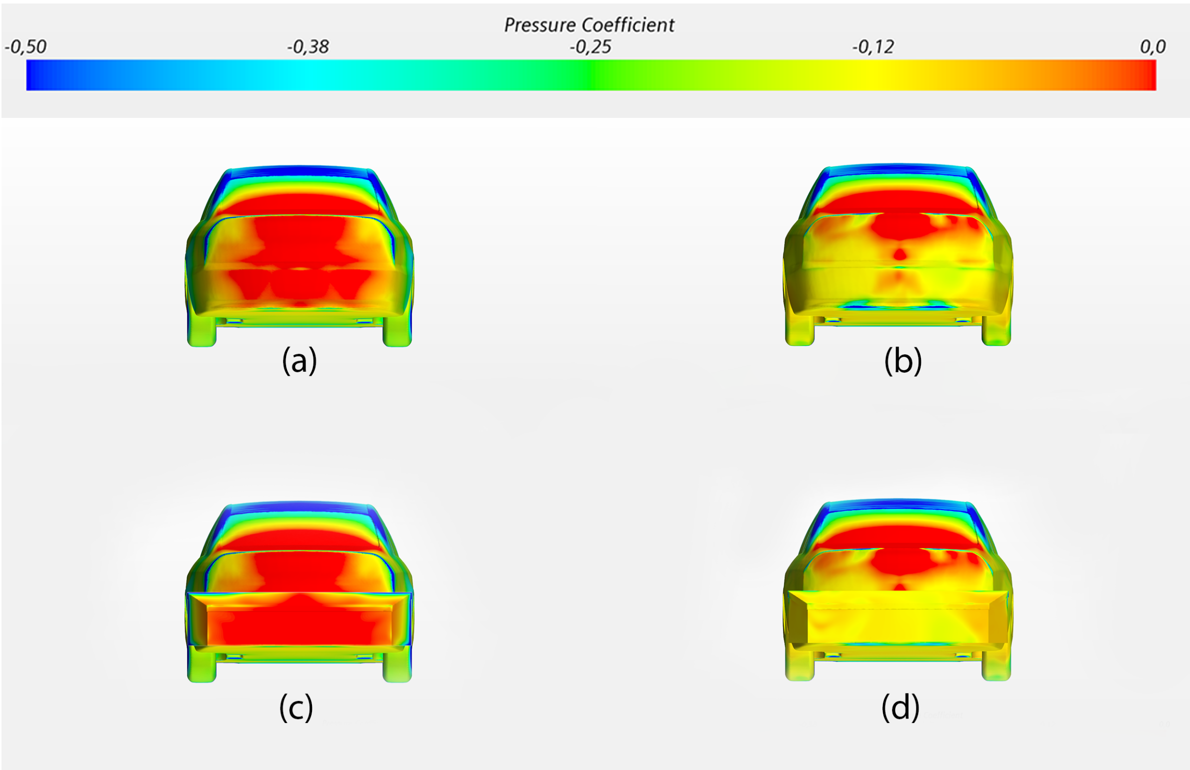

Figure 5.7: C_p *plots of 170-40 box. (a) is using RKE and show pressure recovery on the car, without the IXTAbox visible,(b) is using* $k-\omega$ *and show pressure recovery on the car, without the IXTAbox visible, (c) is using RKE where the IXTAbox is visible, (d) is using* $k-\omega$ *where the IXTAbox is visible.*

While the pressure recovery on the car is aided by the IXTAbox, stagnation occur on the box itself, giving a negative net contribution to C_dA. As seen in figure 5.8 there is a strong stagnation in the middle section of the IXTAbox, where air coming from the underbody is captured by the box, on the other hand, depending the degree of flow separation that each turbulence model predict, stagnation also occur on the side as for the case using RKE. What should also be noted is that on the sections where no stagnation occur, the pressure distribution is similar to what each turbulence model predict on the trunk of the car, with a slightly negative value using $k-\omega$.

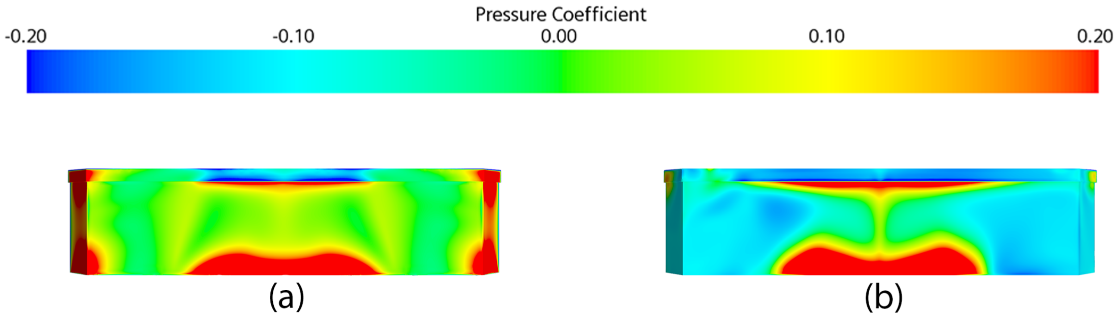

Figure 5.8: C_p *plots of 170-40 box. (a) is using RKE and show stagnation on the IXTAbox surface facing the car, (b) is using* $k-\omega$

When it comes to how the turbulence models differ from each other, each on their own share many similarities when using the same turbulence model as in in the reference base only using *DrivAer*. For example, using *RKE* the geometry of the pressure recovery on the trunk, is observed to be similar to that of only using *DrivAer* but more intense. The same applies to when using $k-\omega$ with its evenly distributed pressure recovery of roughly -0.12 when only using *DrivAer* which is also seen when putting on the 170-40 box as in figure 5.7.

Moving on to show the wake development through C_{ptot}, in two set of planes for each turbulence model, the first plane, will be 0.1m away from the car, the exact same plane shown in 5.1 and should be compared to the images presented there. However with the IXTAbox implemented, this plane lies between car and box. To show the development of the wake when using the IXTAbox, another plane that lies 0.1m away from the IXTAbox, or 0.2 m away from the car. In figure 5.9 these plots are shown.

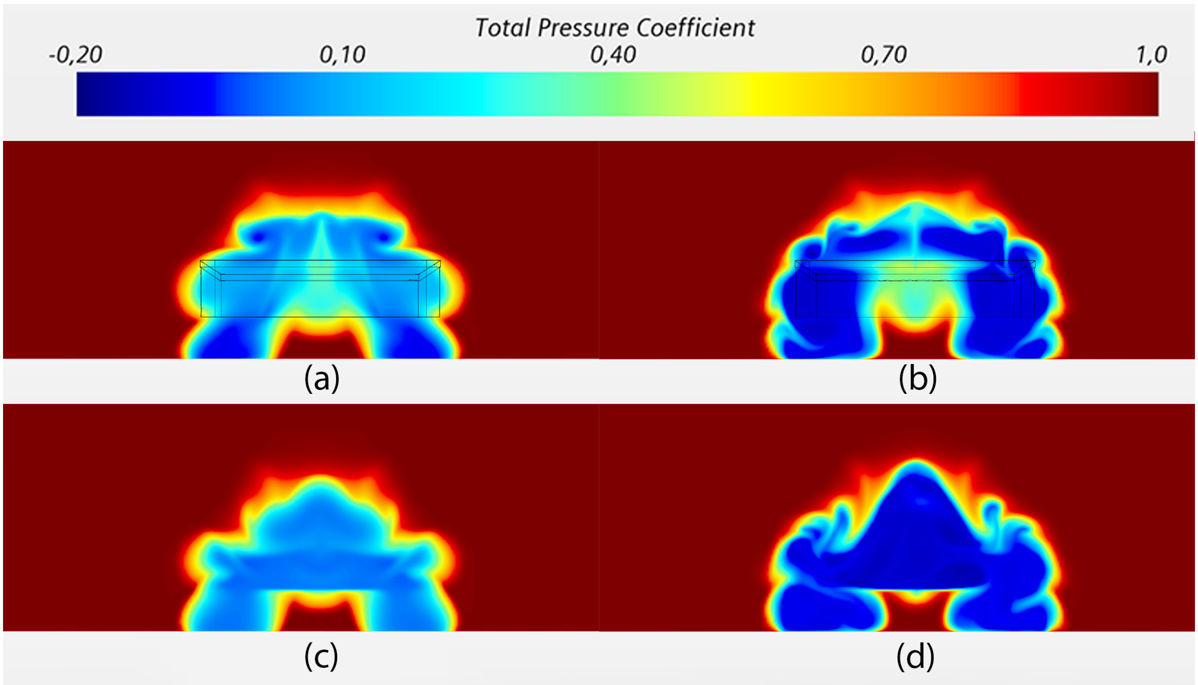

Figure 5.9: C_{ptot} *plots of 170-40 box. (a) is using RKE and is 0.1m away from the car,(b) is using* $k-\omega$ *and is 0.1m away from the car, (c) is using RKE and is 0.1m away from the IXTAbox, (d) is using* $k-\omega$ *and is 0.1m away from the IXTAbox.*

When comparing the images in 5.9 to 5.3 it is noted for RKE that the pressure distribution coming from the wheels are similar, however a pressure increase can be seen in 5.9 in the middle of the IXTAbox where flow from the underbody is changing flow direction to the Z-axis through the shoveling of air that the IXTAbox does on the flow which is not the case in 5.3. Furthermore it appears that when using the IXTAbox, the area where C_{ptot} is less than one, is larger when using the IXTAbox, thus a larger wake structure can be concluded. This increase of wake area comes from the fact that the box capture separated flow and forces it around the box, such as on the sides and bottom. On the other hand, the overall intensity of the wake is less compared to when only using *DrivAer*. When comparing $k-\omega$ in 5.9 to 5.3, a pressure increase in the middle parts of the IXTAbox is observed just as when using RKE, the intensity of the increase is of course coupled to the pressure recovery on the surface as seen in 5.7. Moving on, comparing the wake $0.1m$ away from the IXTAbox, both models predict the low pressure zone after the IXTAbox, an area whose geometric wake structure is influenced by the IXTAbox's flat surfaces, which is for example observed just above the high pressure zone in the lower, middle part of the images in figure 5.9. Lastly, it seems like small vortexes are predicted in $k-\omega$ not seen in RKE such as on each side of the IXTAbox, it is most likely that this is induced drag where "wingtip" vortices are created, as the wake structures are somewhat different, only $k-\omega$ captures them.

When comparing the streamlines for the two turbulence models, many features that were observed in the reference case only using *DrivAer* can be seen. For RKE much of the flow that separates at the side of the trunk, are drawn into the large formation in the middle while for $k-\omega$ the flow that separates on the side, flow over the box into the two large vortices leaving the box on the side. With this in mind, one can conclude that the choice of turbulence model, and how it predicts the flow separation will have an affect on C_d as the pressure recovery on the surface, and the stagnation point that forms on the IXTAbox surface that is facing the car are dependent on how the flow is directed around the box.

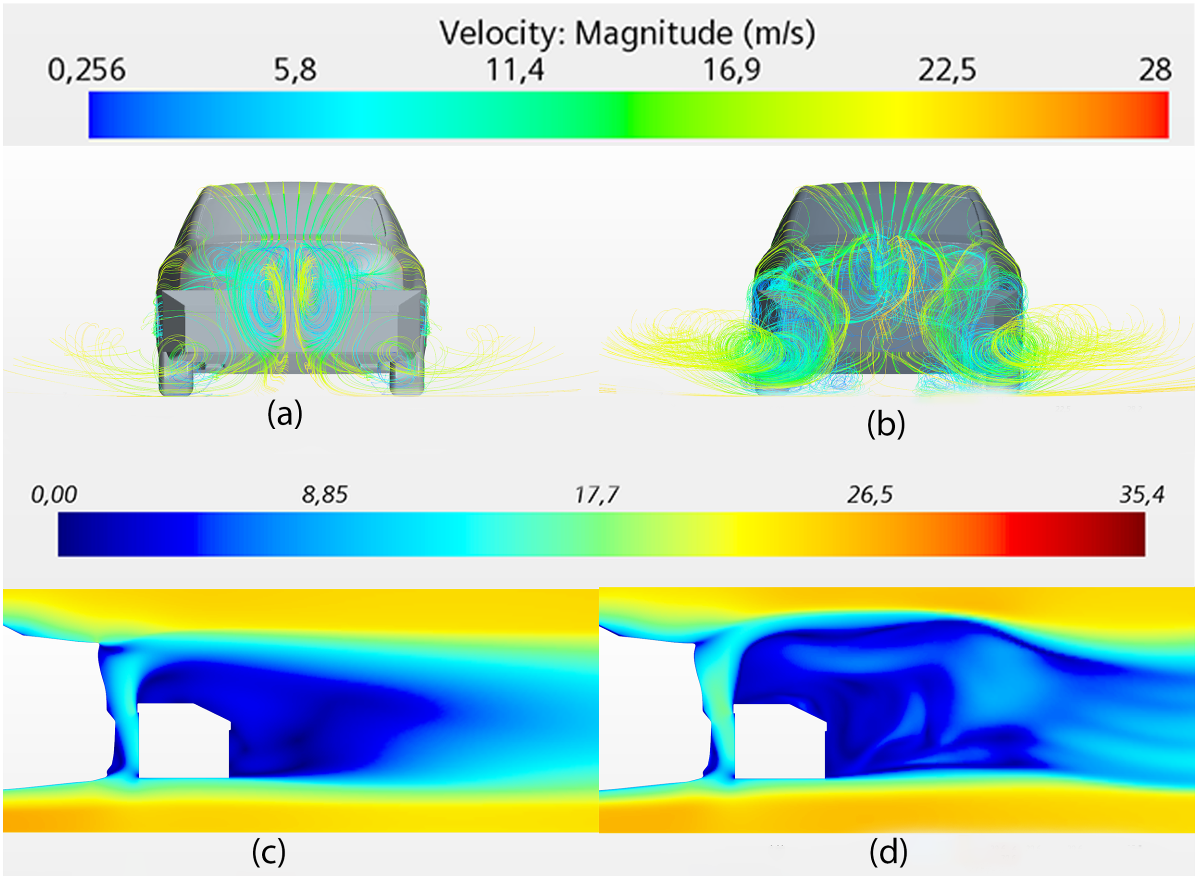

Figure 5.10: *Velocity plots of 170-40 box. (a) is using RKE from the top,(b) is using $k-\omega$ from the top, (c) is using RKE along the symmetry, (d) is using $k-\omega$ along the symmetry. The upper color bar is for (a) and (b) while the middle color bar is for (c) and (d)*

The velocity magnitude plot in figure 5.10, also shows how the IXTAbox shovel air from the underbody to be mixed with air coming from the top, this is the largest source of turbulence for the IXTAbox, which decrease the pressure recovery over the IXTAbox. Due to this shoveling phenomena, the equilibrium between upwash and downwash which is balanced for the car itself, moves due to the increase of upwash due to the box. This can be seen as the wake is pushed up, compared to the reference case. Furthermore, it is seen that the wake in $k-\omega$ is more irregular, and explains why its residuals, and force monitors have a periodic solution, since it seems harder to find steady state when using $k-omega$. As noted in the theory section, turbulence is highly irregular, and unsteady. The steady solver forces the turbulence to a steady state solution, but this cannot always be found. Adding the IXTAbox to the wake seems to be a borderline case, where RKE failed for the boxes of height 60 which is seen in section 5.4.

5.3.2 Boxes of height 60

As RKE failed to predict the correct and expected flow phenomena when the boxes were $60cm$ high. Only $k-\omega$ can be used. The three different boxes will be compared to each other and compared to $DrivAer$ using $k-\omega$ which forms the reference case.

When it comes to the pressure recovery of the large boxes, it can be seen once again that the impact of the IXTAbox is only on the trunk, where in increase the pressure recovery, at the cost of a stagnation area on the face of the box that is against the car. As the box of height 60 captures much more flow that separates from the trunk, such as on the side of the car, the stagnation area has increased. At the same time, a larger surface of the IXTAbox is now facing a slightly negative pressure coefficient as seen in figure 5.11

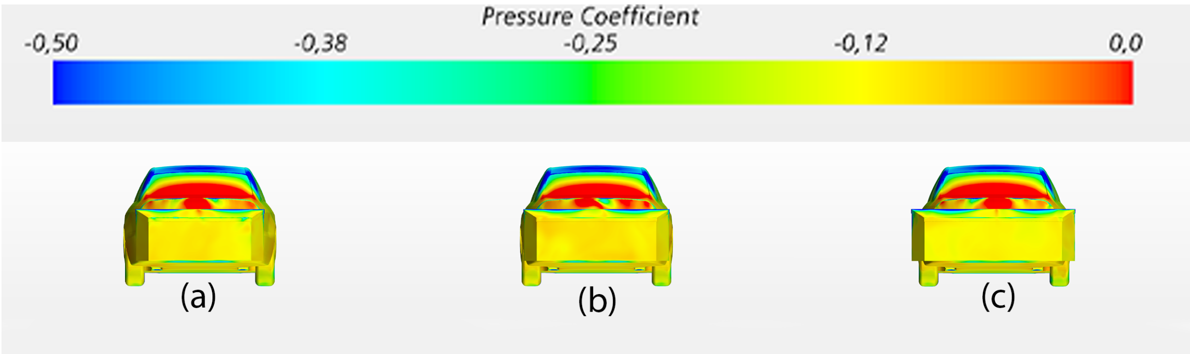

Figure 5.11: *C_p plots over the IXTAboxes of height 60 using $k-\omega$, (a) is the 150-60 box, (b) is the 170-60 box and (c) is the 190-60 box*

Moving on to the pressure on the IXTAbox surface facing the car. It can be seen that the stagnation that occur in the middle section of the box as seen in figure 5.12 share a similar area, explaining why the C_d is similar for boxes of height 60 using $k-\omega$. Here can can note that the 190 box, and to some extent have some pressure increase/stagnation on the sides where they capture some of the flow.

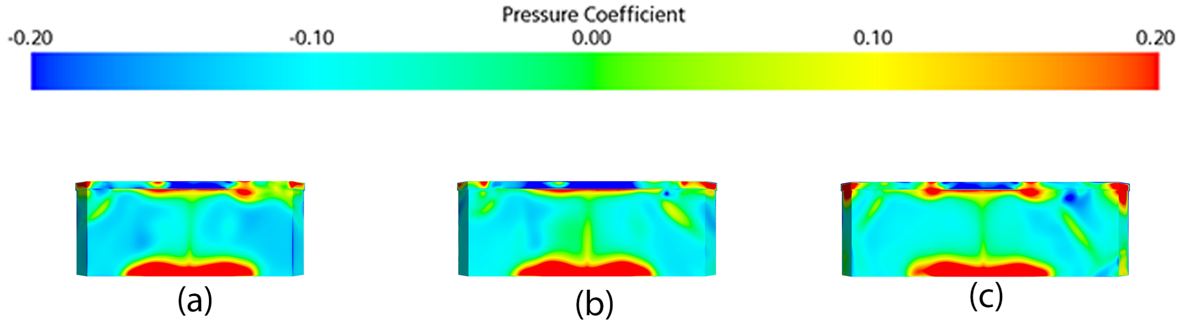

Figure 5.12: *C_p plots for the surface facing the car, for IXTAboxes of height 60 using $k-\omega$, (a) is the 150-60 box, (b) is the 170-60 box and (c) is the 190-60 box*

All these attributes to an increased value of C_d as well as C_dA as both the 170-60 and 190-60 is not entirely covered by the car, which the other 4 IXTAboxes are. However, the increase of C_d for the boxes of height 60 is minimal, which is not the case for the boxes of height 40. This is likely due to the fact that the boxes of height 60 capture almost the same amount of separated flow from the sides, while the increase to C_d is attributed to the larger surface area of the part surface facing the wake in the X-direction.

In figure 5.13 one can see how the boxes capture the same type, and amount of separated flow from the trunk, never mind which box is used. The total pressure coefficient plots are almost indistinguishable irregardless of the width. What is also interesting is when comparing the 60 boxes to a 40 box, is that what almost looks like a moustache, for lack of better wording in 5.9 just above the roof of the IXTAbox is no more for the 60 boxes, instead the flow is forced along the wall until it hits the flow from the top of the car. This gives further proof to the hypothesis that the flow coming from under the car is the most critical parameter since it influence the stagnation on the box surface. The three images in figure 5.13 that is in the Z-plane 0.1m after the boxes are very much influenced by the shape of the box, as there is a straight line along the horizon that stems from the bottom part of the IXTAbox. This shape is stronger and larger than for a 40 box shown in figure 5.9, finally one can distinguish the formation of one large middle vortex due to the flow coming from between the box and car mixes with the flow coming from the top, as well as smaller vortices likely due to induced drag for the flow that moves over the IXTAbox, which can be verified in figure 5.14 as well.

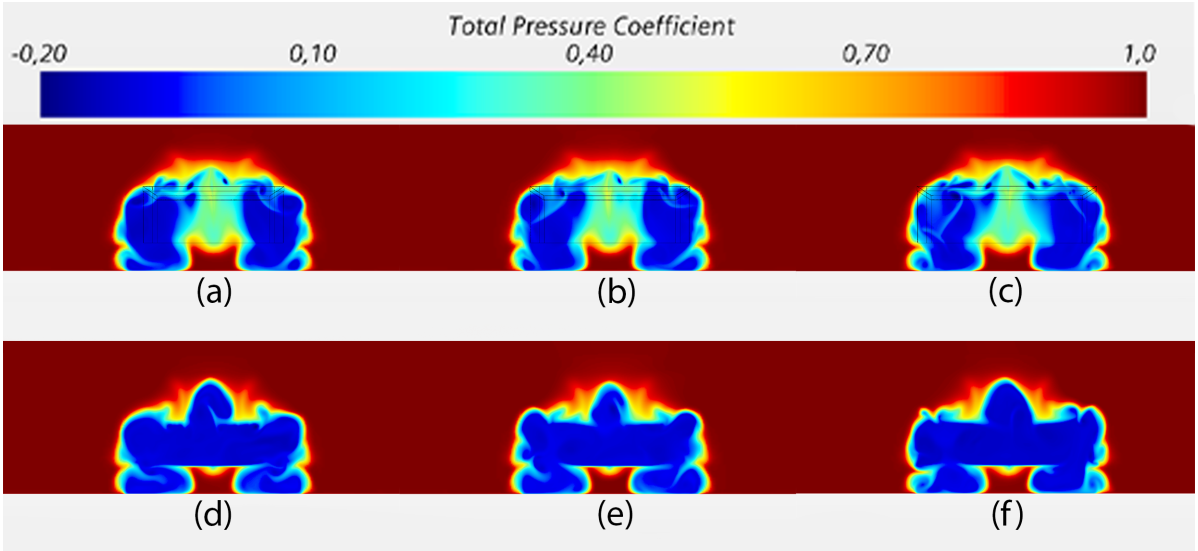

Figure 5.13: C_{ptot} *plots of boxes of height 60 using* $k-\omega$. *(a) is the 150-60 box 0.1m away from the car,(b) is the 170-60 box 0.1m away from the car, (c) is the 190-60 box 0.1m away from the car, (d) is the 150-60 box 0.1m away from the IXTAbox, (e) is the 170-60 box 0.1m away from the IXTAbox, (f) is the 190-60 box 0.1m away from the IXTAbox*

When comparing the streamlines from behind in figure 5.14, one can note that the flow coming from the side of the car splits to flow either on the roof of the box, the side of the box, or along the box in the along the y axis. The flow that splits over the roof or side of the box, will in the wake combine into the large vortex seen on the side behind the box. The flow that is pulled to the middle parts of the car, mixes with the flow coming from the underbody and top to form the middle wake structure.
In figure 5.14 it is noted that when looking at the velocity magnitude from the side, the small separation vortex at the diffusor of the car is compressed compared to 5.10 and that the velocities are higher between the box and car compared to 170-40. Furthermore, its not a clean separation for the vertical flow as the separation point for the vertical flow between car and box is much closer to the flow coming from the top trunk, compared to the 170-40 box.

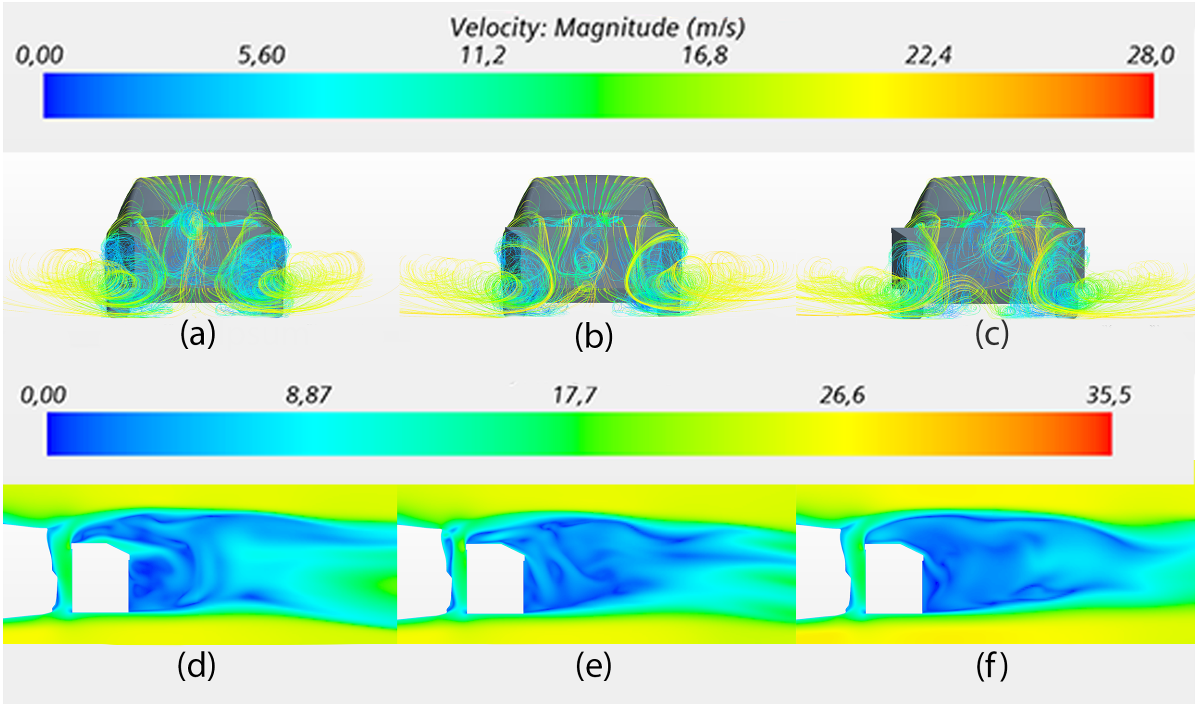

Figure 5.14: *Velocity overview for the boxes of height 60 using* $k-\omega$*. (a) is the 150-60 box using streamlines, (b) is the 170-60 box using streamlines, (c) is the 190-60 box using streamlines, (d) is the 150-60 box in the XZ-plane for Y=0 using velocity magnitude, (e) is the 170-60 box in the XZ-plane for Y=0 using velocity magnitude,(f) is the 190-60 box in the XZ-plane for Y=0 using velocity magnitude. Sub figure (a), (b) and (c) use the top color bar while (d), (e) and (f) use the middle color bar.*

5.3.3 Boxes of Height 40

This section will present the last two boxes and should be compared to the 170-40 box and DrivAer using *RKE*. For the case of pressure recovery on the trunk, it can be seen in figure 5.15 that it is the size of the IXTAbox that dictate the pressure recovery on the car itself, on the other hand the larger the box, the large the stagnation on the box's surface facing the car as seen in figure 5.16. Which can be concluded by comparing all three boxes by observation of the pressure coefficient in figure 5.15 and 5.7.

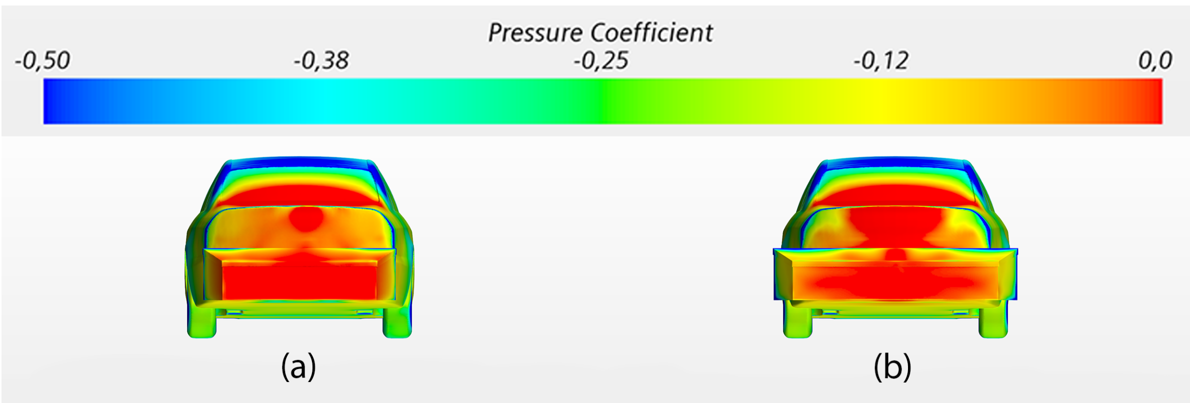

Figure 5.15: C_p *plots over the IXTAboxes of height 40 using RKE, (a) is the 150-40 box, (b) is the 190-40 box*

Moving on to show the stagnation on the surface of the IXTAbox facing the car, once again the stagnation in the middle plays an important role towards the power increase as the pressure increase on a surface facing the driving direction. As RKE predicts the flow coming from the sides in a different manner than $k-\omega$, more stagnation occur on the box if it is wide enough, something that the 190 box does.

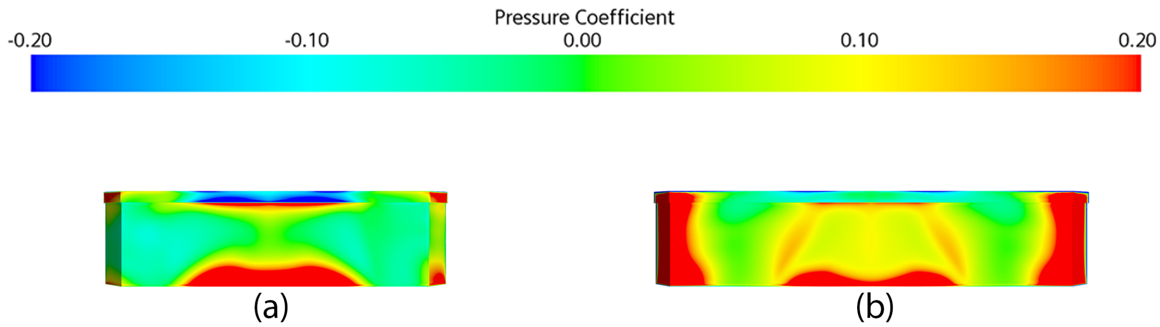

Figure 5.16: C_p *plots for the surface facing the car, for IXTAboxes of height 40 using* RKE*, (a) is the 150-40 box, (b) is the 190-60 box*

When it comes to total pressure coefficients in figure 5.17, to show the wake development in can be seen that RKE predicts that the flow that is captured on the sides of the IXTAbox is strong enough so that minimal amount of flow is allowed between the car and IXTAbox.

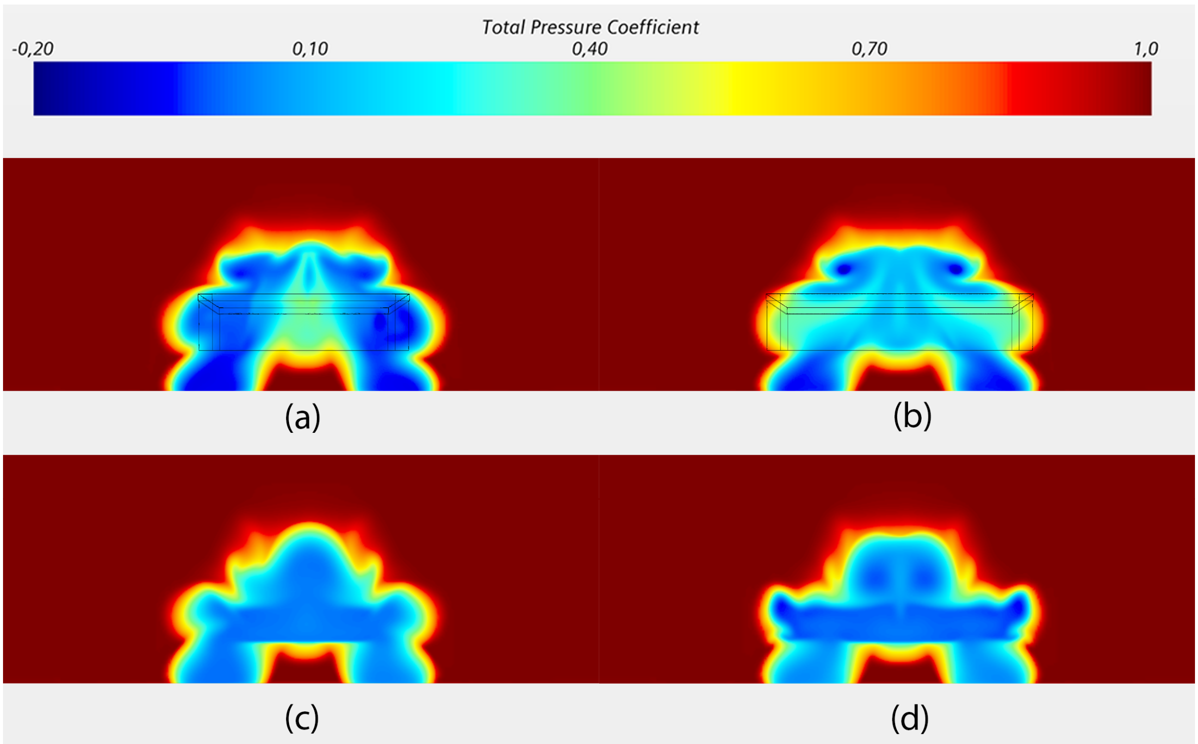

Figure 5.17: C_{ptot} *using* RKE*. (a) is the 150-40 box 0.1m away from the car,(b) is the 190-40 box 0.1m away from the car, (c) is the 150-40 box 0.1m away from the IXTAbox, (d) is the 190-40 box 0.1m away from the IXTAbox.*

This can be seen due to the fact that the middle section in figure 5.17 for the 190-40 box have a lower pressure in the middle, than on the side, a phenomena that is flipped for the 150-40 and 170-40 box. This also explain why the difference of C_d for the turbulence models differ for the 190-40 box, while they are more similar for the 150-40 and 170-40 boxes. Moving on to the total pressure coefficients behind the

IXTAbox in figure 5.17, the wake formed is similar for all three boxes of height 40 using RKE, the main difference is that the width of the box, determines how wide the wake formed is.

Many similarities are found when comparing the streamlines of the 150-40 box in figure 5.18 to that of the DrivAer without any box. As the box is not as wide as the two wider boxes, its influence on the flow coming from the sides are low and is proved since the streamlines flowing along the side of the car, for both 150-40 and DrivAer share similar scales, magnitudes and direction for the streamlines plot that use the exact same settings. This is not the case for the 190-40 box that is slightly wider than the vehicles itself. Here, one can see how the box captures the flow along the sides and forces it to the middle, in the area between the box and the car's back. Which on the other hand was already proved by observation of the total pressure coefficient.

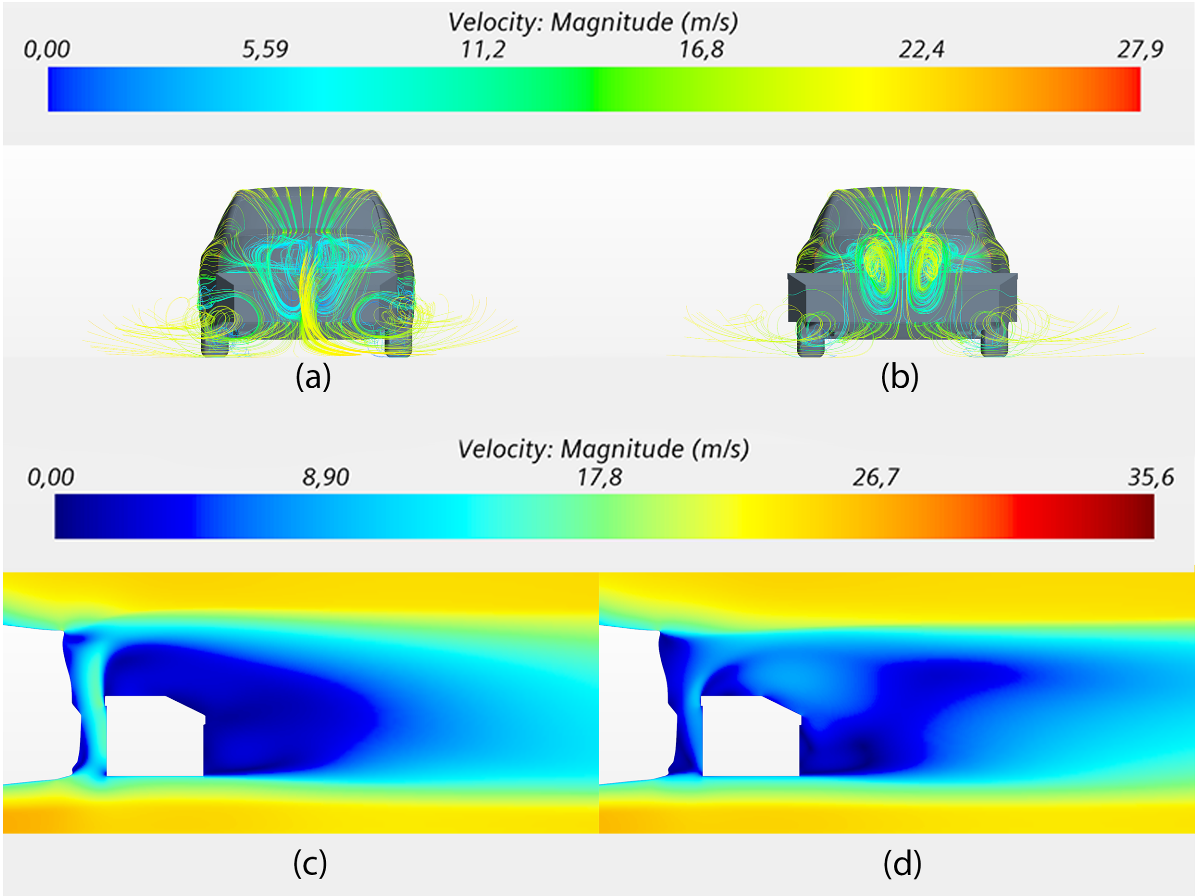

Figure 5.18: *Velocity plots using streamlines seen from the back, and velocity magnitude in the wake of the car in the symmetry plan using RKE (a) shows the 150-40 box streamlines,(b) shows the 190-40 box streamlines (c) is the 150-40 box along the symmetry, (d) is the 190-40 box along the symmetry. The top color bar is for sub figure (a) and (b) while sub figure (c) and (d) use the middle color bar.*

This capturing of air influences how much air is coming from below, as the air coming from the side pushes away the air coming from below. Looking at the velocity plots from the side in figure 5.18, there is a stark difference between the velocity magnitudes between the 150-40 and 190-40 boxes. However, using $k - \omega$, flow from under the car shares similar flow phenomena as the 150 box. As not as much flow is coming from under the box for the 190-40 box when using RKE the flow flowing on the top of the car forms two strong vortex structures while the vortex structures usually formed on the sides are of much less strength as seen in figure 5.18

5.4 Failure of RKE to predict the flow for the large boxes

Throughout this thesis, it has extensively been repeated how two turbulence models have been used, this is due to the fact that RKE failed to predict the correct flow for the boxes of height 60, which will be discussed here. Here, one should note that the 190-40 box case carries some of these problems as well. However, some flow is coming from the underbody, which could explain why ΔC_d is higher between the turbulence models than for the other two boxes of height 40, *DrivAer* or roof boxes.

What is happening in the case for RKE on the boxes of height 60 is that the space between box and car predicts that much of the flow that is separated behind the trunk, is captured by the box as it covers almost the whole trunk. This create a wake that is much harder for RKE to model correctly as each flow is pushing against the other three. For the boxes of height 40, they only capture the flow coming from below which make the balance much easier to solve.

This mean that that highly asymmetrical solutions are found for 190-60 and 170-60. 150-60 box on the other hand have symmetrical solutions as seen in figure 5.19 and have a C_d value close to the solution found using $k-\omega$. However, no flow is coming from the underbody up through the space between box and car even for the 150 box which is predicted using the box of height 40, or by using $k-\omega$. For the 170-60 and 190-60 boxes, which have a C_d value up to 40 counts higher due to their highly asymmetrical solutions it is deemed that the model fails completely. On the other hand, $k-\omega$ achieves a symmetrical solution and where the flow coming from the underbody is predicted to be the dominant flow.

In figure 5.19, one can observe how a large vortex is formed for the 170-60 and 190-60 cases. It almost looks like a side wind simulation is running, which is not valid. When looking at the flow from the side, it can be seen that no flow is coming from the underbody. RKE predicts that the flow coming from one of the sides to be the strongest.

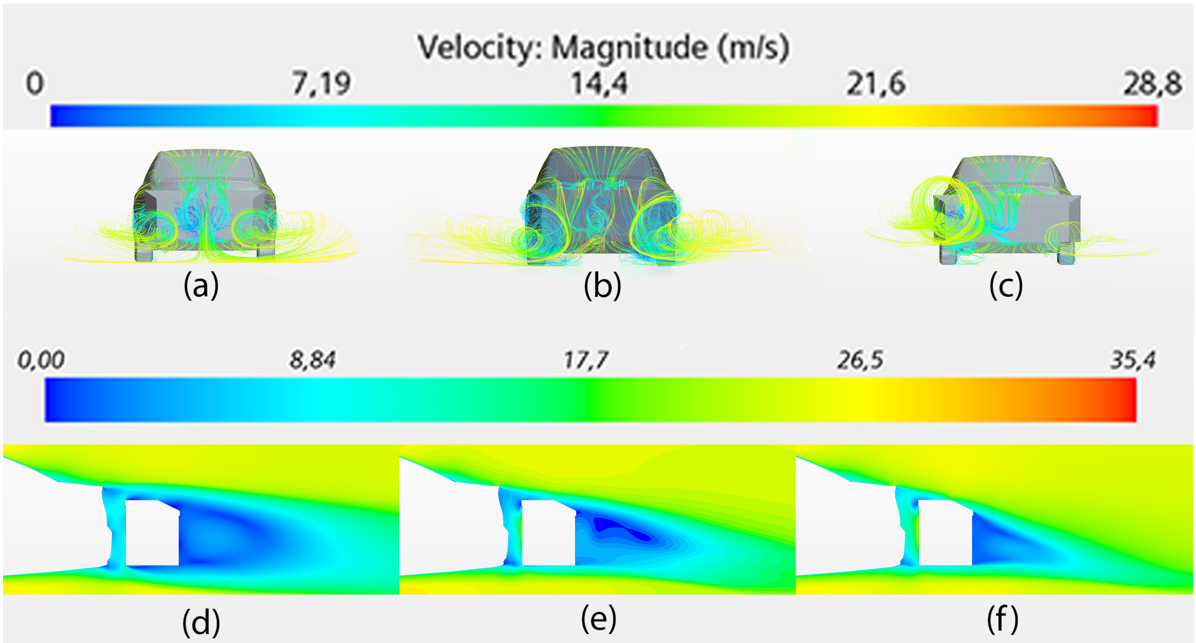

Figure 5.19: *Velocity plots of boxes of height 60 using RKE. (a) is the 150-60 box using streamlines,(b) is the 170-60 box using streamlines, (c) is the 190-60 box using streamlines, (d) is the 150-60 box velocity magnitude for the XZ-plane for Y=0, (e) is the 170-60 box velocity magnitude for the XZ-plane for Y=0, (f) is the 190-60 box velocity magnitude for the XZ-plane for Y=0. The top color bar should be used for sub figure (a), (b) and (c) while the middle color bar should be used for sub figure (d), (e) and (f)*

With this in mind, and the fact that the C_d difference between RKE and $k-\omega$ is over 40 counts for the

190-60 box. RKE is said to have failed to predict the flow correctly. It should also be said here that a mesh study have been conducted where additional volumetric refinements around the box was done. By looking at the solution, the most obvious error was to double check if the box extends the same amount in the $\pm Y$ so that its middle coordinate lies in the plane $Y = 0$ which it does. ´

5.5 Height Variations of Ixtabox

The IXTAbox comes with the possibility to vary its height in reference to the ground to make it more versatile for various cars. Two additional experiments were conducted to gain more insights into the flow around the Ixtabox and get data on C_d impact when varying the height. The reference has a height above the ground set to 30 cm, however, two more additional experiments were conducted where 26 cm and 22 cm above the ground was decided. In table 5.2 on can see the reported C_dA values.

Table 5.2: Reported C_dA values when varying the height above the ground

Height Above Ground(cm)	C_dA
22	0.577
26	0.560
30 (Reference)	0.556

Analysing the flowfield as seen in figure 5.20 the difference between the base-case of 30 cm above the ground and 26 cm above ground is almost negligible, verified by a small increase in C_dA as seen in table 5.2. The impact can for example be seen that the small circulation zone at the diffusor in the reference case is removed as the massflow have increased between box and car in the 26cm case. However moving down to 22 cm above ground gives a larger, nonlinear addition to C_dA. This means, first of all, that height is a sensitive parameter, second of all it verifies that the largest C_d addition to Ixtabox compared to only having the car comes from the fact that Ixtabox "shovels" air coming from the underbody and forces it upwards, giving rise to a larger stagnation point on the box surface facing the car. Furthermore, the more air that is shovelled, the more turbulence is created when the two flows mix, and thus a loss in pressure recovery - which induce drag.

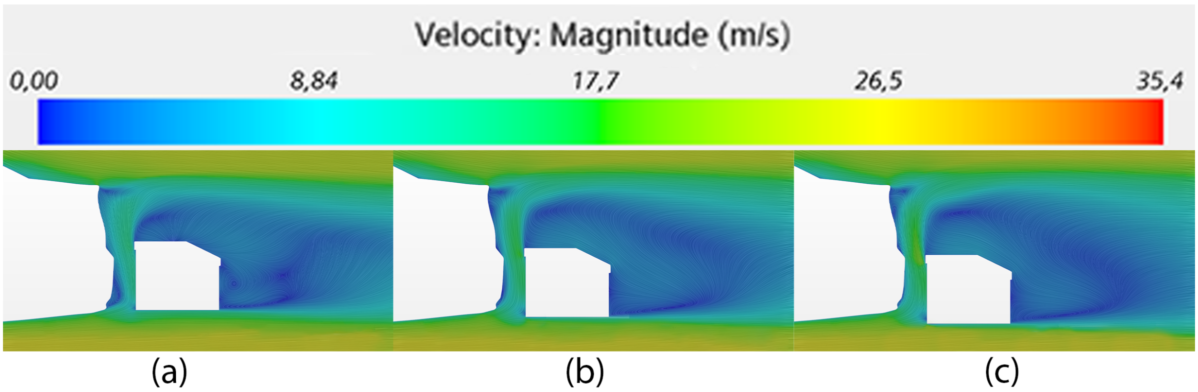

Figure 5.20: *Height variations for 170-40 box, one can observee how the flowfield for 30 cm and 26 cm above ground are similar while the case for 22 cm above ground have larger wake, and faster flow going between car and box. Image (a) corresponds to 30 cm abouve ground, (b) is 26 cm while (c) is 22 cm above ground*

At 30 cm above ground, the bottom of the IXTAbox have almost the same Z-plane as the topmost part of the diffusor on the car, 26 cm is just below the topmost part while 22 cm is at the same Z-plane as the bottom of the diffusor. As diffusors have different parameters for different cars, this is of course, something to consider, however, further analysing the wake for notchback DrivAer, the wake volume is larger when Ixtabox is at 22 cm above ground, as the upwash from the diffusor is more potent than the intended downwash. Additionally, the diffusor on the car loses its intended purpose to slow down and expand the air coming from the underbody. It instead sets the direction for more air to pass upwards between the car and the Ixtabox to mix with the downwash. With this in mind, the relationship between diffusor and IXTAbox is an important one, where much of the aerodynamic improvement can be found as well as serve as a warning so that one doesn't place the IXTAbox too low for their respective car model as more air will stagnate on the IXTAbox's surface.

5.6 IXTAbox aerodynamic improvements on the 170-40 box

As in the beginning of the results chapter, an amuse bouche will be presented in the form of a table, to give an overview to the 11 improvements studied. Then each improvement will be discussed, the 4 most successful ones more extensively than the non successful ones. As there is a time constraint to the thesis, it was deemed most interesting to study the sensitivity of various improvements, rather than study one improvement and iterate it in order to gain a optimised design. In the table below one can see the C_dA values obtained from the aerodynamic improvements, to be further discussed below.

Table 5.3: Overview over the aerodynamic improvements studied

Type of Improvement	C_d	**Area**(m^2)	C_dA
Diffusor Extension L	0.248	2.106	0.522
Diffusor Extension S	0.250	2.106	0.527
Vortex Stabiliser	0.256	2.106	0.539
Arc Diffusor	0.260	2.106	0.548
Z-Baffles	0.261	2.106	0.550
Straight Diffusor	0.262	2.106	0.552
Side Panels 20cm	0.263	2.106	0.554
X-Baffles	0.263	2.106	0.554
Rounded Edge	0.263	2.106	0.554
170-40	0.264	2.106	0.556
Side Panels 10cm	0.264	2.106	0.556
Teardrop	0.269	2.106	0.567

When running the six IXTAboxes in the base case, many conclusions could be drawn in what happens to the wake when introducing a large object in it. Valid for all IXTAboxes is a flow between the car and IXTAbox of high velocity that mixes with the flow coming from the top of the car producing turbulence. Furthermore, it has been concluded that height variations of the IXTAbox can drastically increase C_d when it shovels more and more air upwards, the lower the IXTAbox is to the ground. This is a strong indication that most of the C_d reductions can be found in optimising the flow between the flow coming from the car's underbody to IXTAbox. In total, 11 improvements have been studied, of which all the successful ones had some sort of design to influence the flow coming from the underbody. Furthermore, it should be noted only the [170-40] box have been used to study the aerodynamic improvements.

One parameter extensively analysed for the improvements on the box is the turbulent kinetic energy scalar,(TKE). In order to sustain the eddies in the wake, kinetic energy has to be taken from the mean flow and undergo energy transformation in the energy cascade, meaning that it is an easy way to show losses, furthermore it is of very high resolution since most volumes of the flow do not produce much turbulence compared to the wake. Also, one can easily recognise where the largest eddies occur with theory from the energy cascade in section 2.2 as the higher intensity produce larger eddies. Thus all improvements will show the turbulent kinetic energy as a parameter to show flow variations, improvements that have been done on the side of the box is shown from the top, while improvements done to the flow coming from the bottom or the top is shown from the side. In figure 5.21 shows the seven improvements that didn't influence C_d enough to be attractive for implementation due to the addition of interference drag that cancelled out the improvement. However, the four most successful cases will be more extensively studied and have their sections.

Comparing the images in figure 5.21 in alphabetical order. It can be seen that the *Z-baffles* slightly decrease the turbulence on top of the box, aiding pressure recovery. The *X-baffles* on the other hand have no visible impact, which explain why its C_dA value have not changed compared to the reference. Moving on the to the *side panels short* it is seen to decrease the intensity in the region between the back of the car, front of the IXTAbox, as well as the wake behind the car has a decreased intensity of TKE. However, there is an increase to TKE on the sides of the box, where the side panels face the flow, thus the increase and decrease of TKE cancel out the potential gain of C_dA. The same phenomena was observed for the *side panels long* to where gains and losses to TKE are observed.

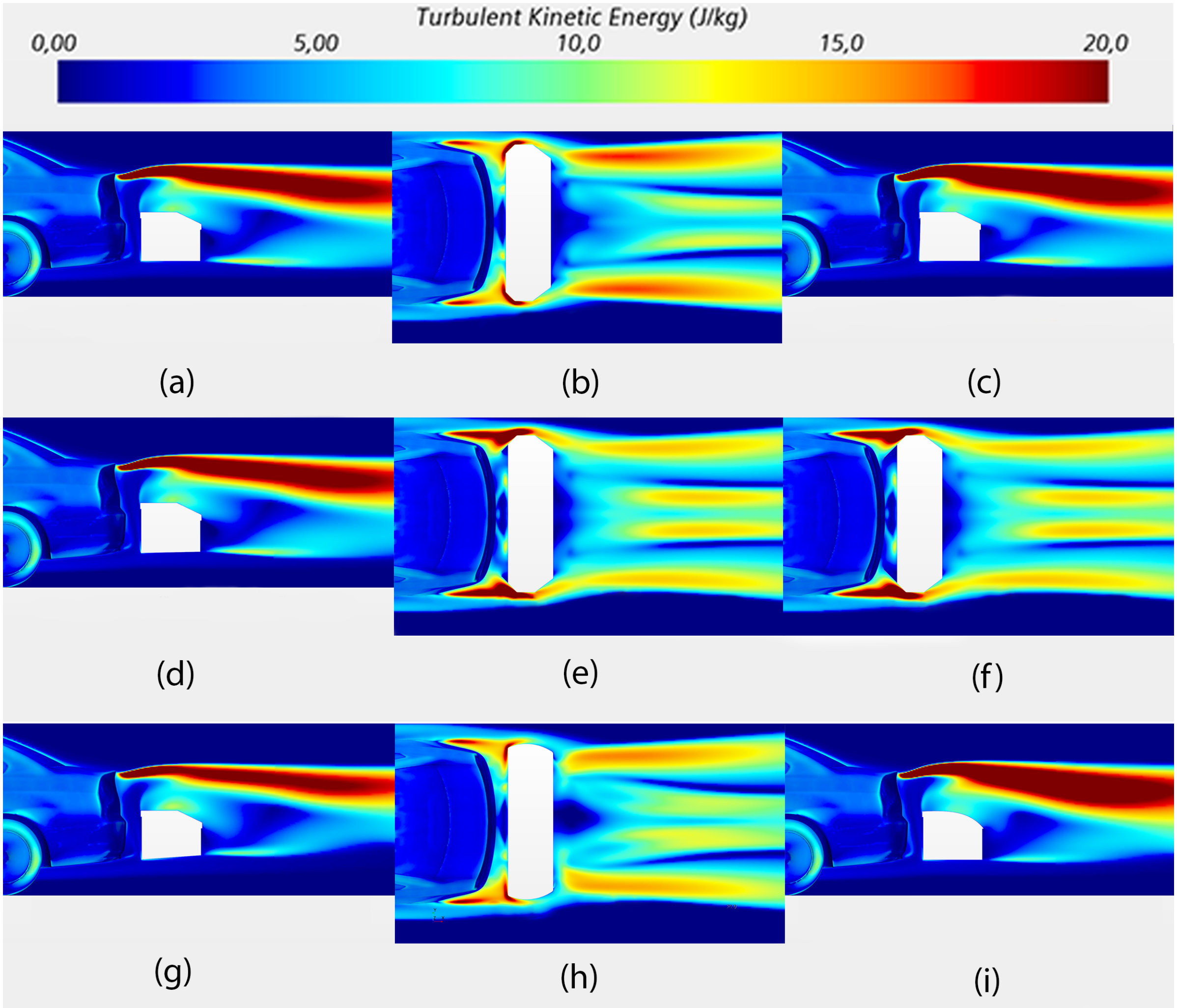

Figure 5.21: *The figure shows where turbulent kinetic energy is taken from the mean flow to sustain the eddies generated from the pressure and flow differences, colliding in the wake. From left to right, top to bottom we have: (a) 170-40 from the side, (b) 170-40 from above, (c) Z-Baffles, (d) X-Baffles, (e)Side panels short, (f) Side panels long, (g) Straight diffusor, (h) Rounded edge, (i) Teardrop*

Moving on to the *straight diffusor*, it can be seen that the turbulence production for the flow leaving the bottom surface of the IXTAbox has decreased compared to the reference, a small reduction in the highly turbulent region above the box is observed as well as the relationship between upwash/downwash is aided by the diffusor on the box. The *rounded edge* improvement was done as flow separation occurs on the sides of the box, which is no longer the case for the rounded edge design through observation of the skin friction coefficient. Despite the removal of this flow separation, only a very small reduction in C_dA is observed. Finally, with inspiration from the trucking industry, a *teardrop* design on the roof of the box was implemented. This was the only improvement that increased C_dA compared to the reference, rather drastically at that coming in at a 5 counts of C_d difference. This is verified by observation of TKE in figure 5.21 as the highly turbulent, red area has increase in volume, worsening the upwash downwash relationship even further.

5.6.1 Diffusor Extension L

The *Diffusor Extension L* is the most successful aerodynamic improvement regarding a reduction of C_dA, the prominent reason being that it allows much of the flow that passes the underbody of the car to continue to pass under the IXTAbox, instead having the box shovel air upwards, which was seen in figure 5.10. Thus the box serves as an diffuser extender which is an aerodynamic device that has been previously studied[11][16] with good results in reducing C_d. In figure 5.22 one can observe how the velocity vectors behave in the wake.

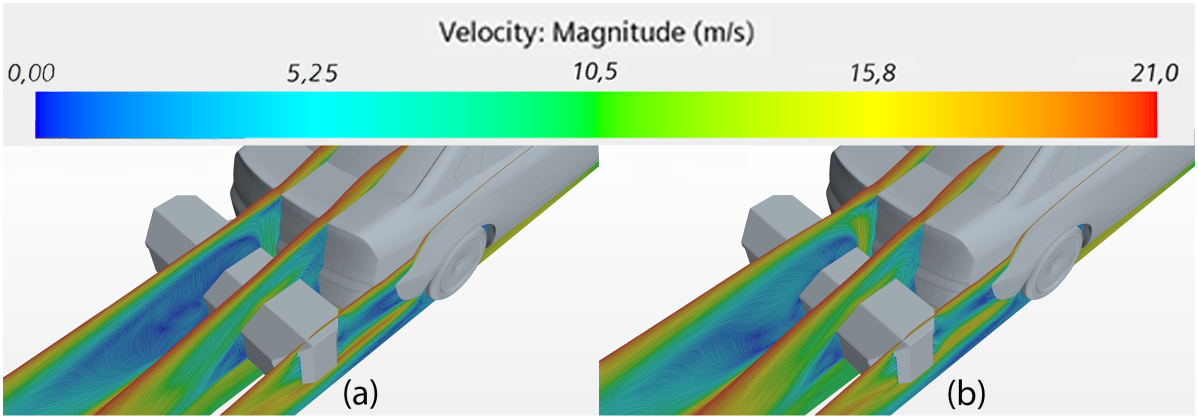

Figure 5.22: *Comparison of wake development for 3 XZ planes with Y values equal to [0,0.2,0.4] where image (a) is the improvement on the 170-40 box while image (b) is the 170-40 to be used as reference*

The first conclusion drawn from figure 5.22 is the fact that the flow coming from the underbody is not entirely sealed, as the extender is placed on the box rather than the car. This small gap allows for some air to pass between the box and the car. However, when comparing the velocity magnitude of the flow coming from the underbody, up between box and car, it is clear that the improvement has a positive influence. Moving on, one can see that on average, the flow velocity in the wake is lower for the improved solution compared to the reference. Comparing the two planes that are 0.2m away from the symmetry, the changes observed are more subtle, the flow field above the roof of the box, for the improved solution, have in general a lower velocity, but no significant difference are observed, the geometry of the flow is similar, this indicates that the extender is the most effective around the middle section of the box, where the wheels do not influence the flow coming from the underbody. For the out most plane in figure 5.22 no differences are spotted at all, further strengthening that statement that a small extender could prove almost as effective.

When comparing the TKE for the *Diffusor Extension L* further information can be done as is done in figure 5.23. The creation of TKE is drastically lower when using the extender, as less flow, and flow of less kinetic energy is allowed to mix with the highly kinetic flow coming from the top of the car. However, one can also observe how there is some production of TKE between the car, and IXTAbox as the gap between the extender and car, disturb the path of the air which is not seen in the base case in figure 5.23.

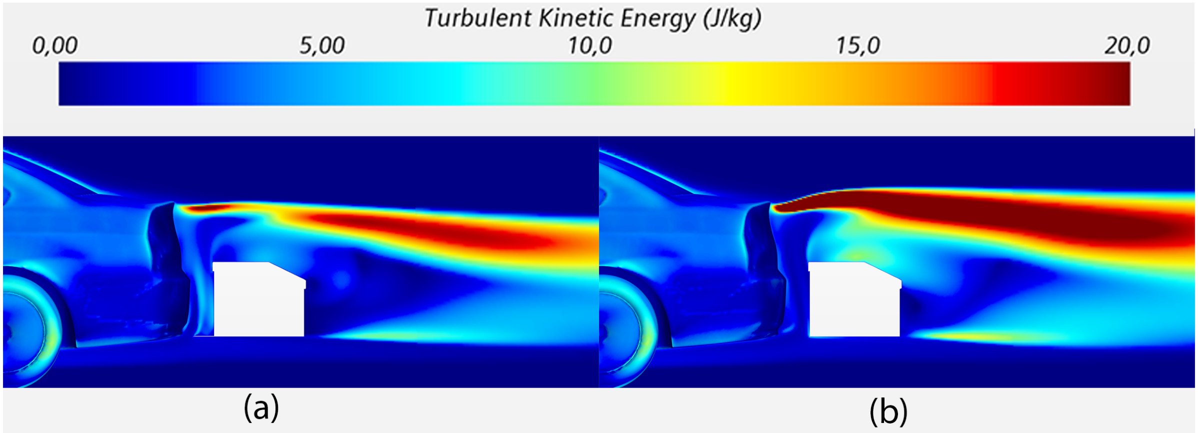

Figure 5.23: *Comparison of TKE for the XZ plane where Y=0 where image (a)is the improvement on the 170-40 box while image (b) is the 170-40 to be used as reference*

It was also discussed how the mean velocity in the wake when using the extender was observed in figure 5.22, this phenomena is also captured above the roof of the box, as less kinetic energy is drawn to produce TKE, as the flow have lower kinetic energy already, or from a pressure perspective, the dynamic pressure is allowed to convert back to static pressure more efficiently when using the extender. Moving on, the production of TKE is also lower for the air leaving the bottom of the box.

When it comes to the pressure coefficient in figure 5.24, a small increase in the pressure recovery on the trunk of the car is observed. especially around the unclean separation at the sides of the trunk. Furthermore on the IXTAbox itself some increase of pressure recovery is observed, especially on the roof of the box. But the largest strength of the extender is that it removes a large portion of the stagnation points on the box's surface facing the car as seen in figure 5.24. Here one can see that the stagnation on the extreme sides of the IXTAbox has decreased as well as in the middle of the IXTAbox. This together with the pressure recovery on the surface facing the wake means that the *Diffusor Extension L* is the most effective improvement studied.

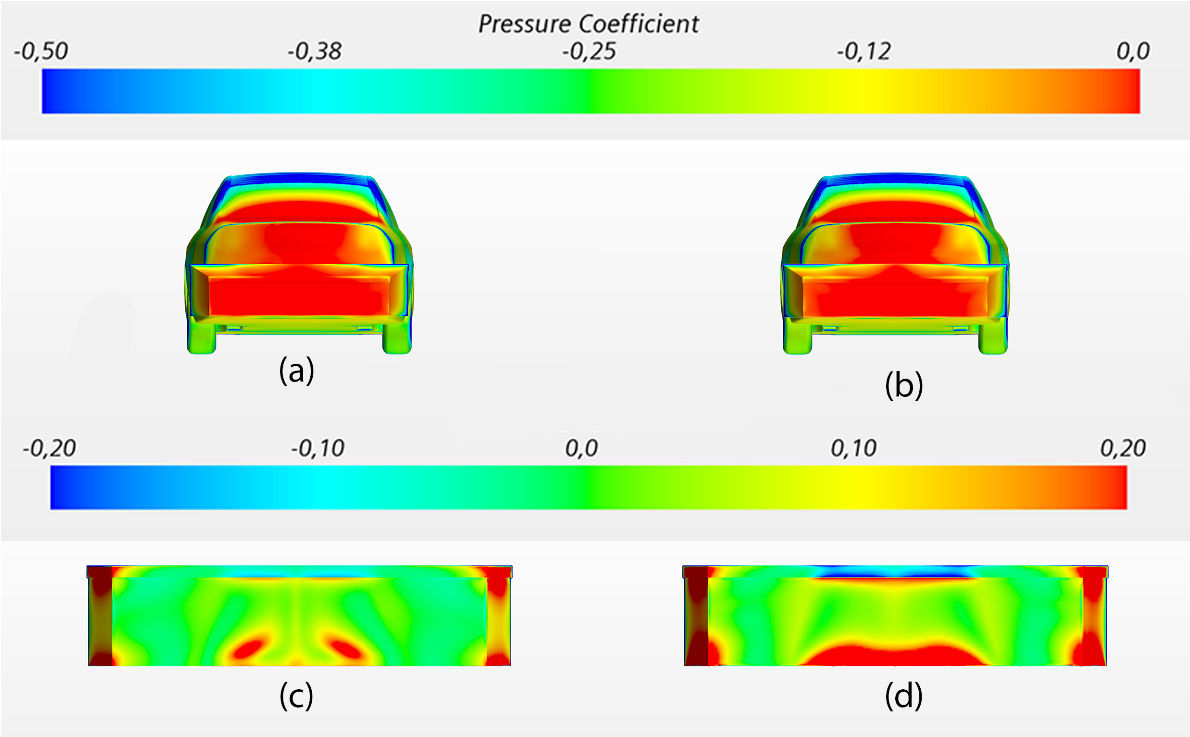

Figure 5.24: *Comparison of C_p on the surfaces of the car and IXTAbox. (a) is the improvement on the 170-40 box from behind (b) is the reference using 170-40 box from behind, (c) is the IXTAbox surface facing the car for the improvement on the 170-40 box, (d) is the IXTAbox surface facing the car for the reference using 170-40. The top color bar is for sub figure (a) and (b) while sub figure (c) and (d) use the middle color bar.*

5.6.2 Diffusor Extension S

One finding that proved interesting in the *Diffusor Extension L* is the fact that indications showed that only the middle part of the diffusor did the critical work, to reduce C_d. To map this sensitivity improvement further, it was also decided to make a smaller extender concentrated on the middle part of the box, this extender, was also much closer to the car, so that the gap was reduced. Comparing the improvement seen in figure 5.25 to that of 5.22, one can see that decreased gap distance decrease the velocity even further for the flow coming up between box and car from the underbody.

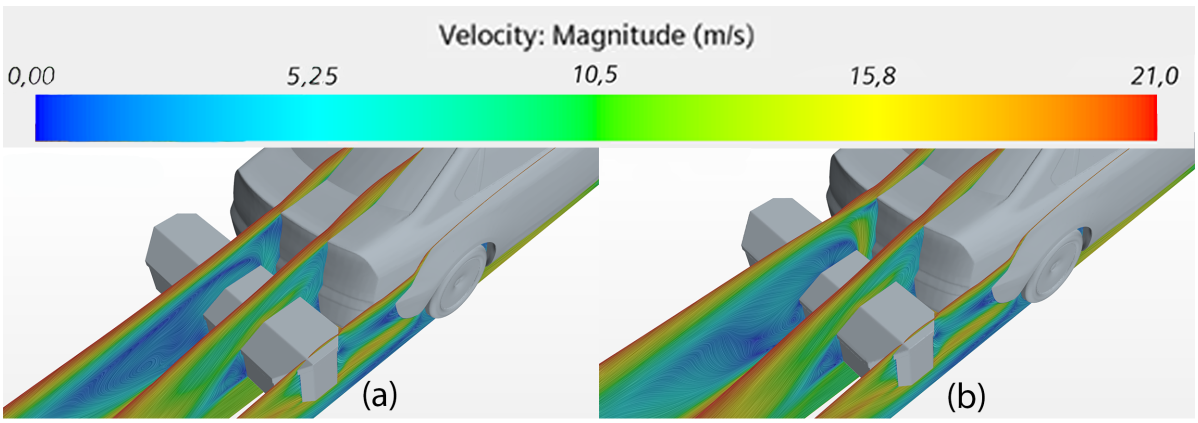

Figure 5.25: *Comparison of wake development for 3 XZ planes with Y values equal to [0,0.2,0.4] where image (a)is the improvement on the 170-40 box while image (b) is the 170-40 to be used as reference*

Moving on the wake plane that is 0.2m away from symmetry, the difference between the reference and the small extender is close to zero, and the same applies to the third wake plane, which indicates that the flow in the Y direction is not affected by the small extender.

When comparing TKE for the small extender in figure 5.26, one can see that even more TKE is produced in the gap between the car and the IXTAbox, compared to the large extender, proving that the gap size influence the turbulence between car and box. On the other hand, almost no TKE is produced at all at the trunk of the car, where underbody and top flow usually meet, clearly depicted in the reference case in figure 5.26 as the decreased gap size, indicate that even less flow is allowed to be shovelled by the box.

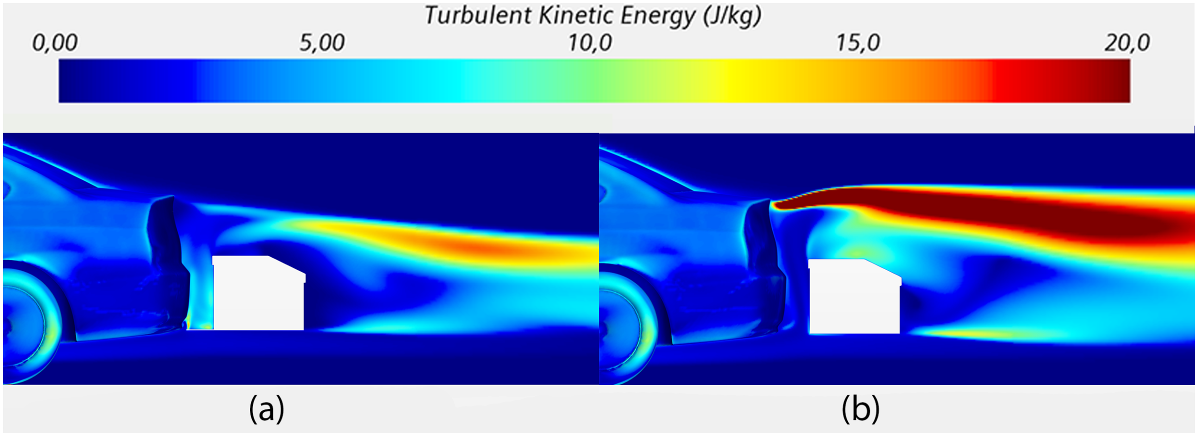

Figure 5.26: *Comparison of TKE for the XZ plane where Y=0 where image (a)is the improvement on the 170-40 box while image (b) is the 170-40 to be used as reference*

Finally, TKE that is produced where the flow separates from the bottom of the IXTAbox has decreased, the extender aid the flow so that flow separation occur much later on the bottom compared to the reference.

Moving on the pressure acting on the surfaces. It can be seen in figure 5.27 that the pressure recovery on the trunk is similar to that of the large extender in the previous sub chapter. The pressure recovery on the top of the IXTAbox is decreased on the other hand compared to the large extender

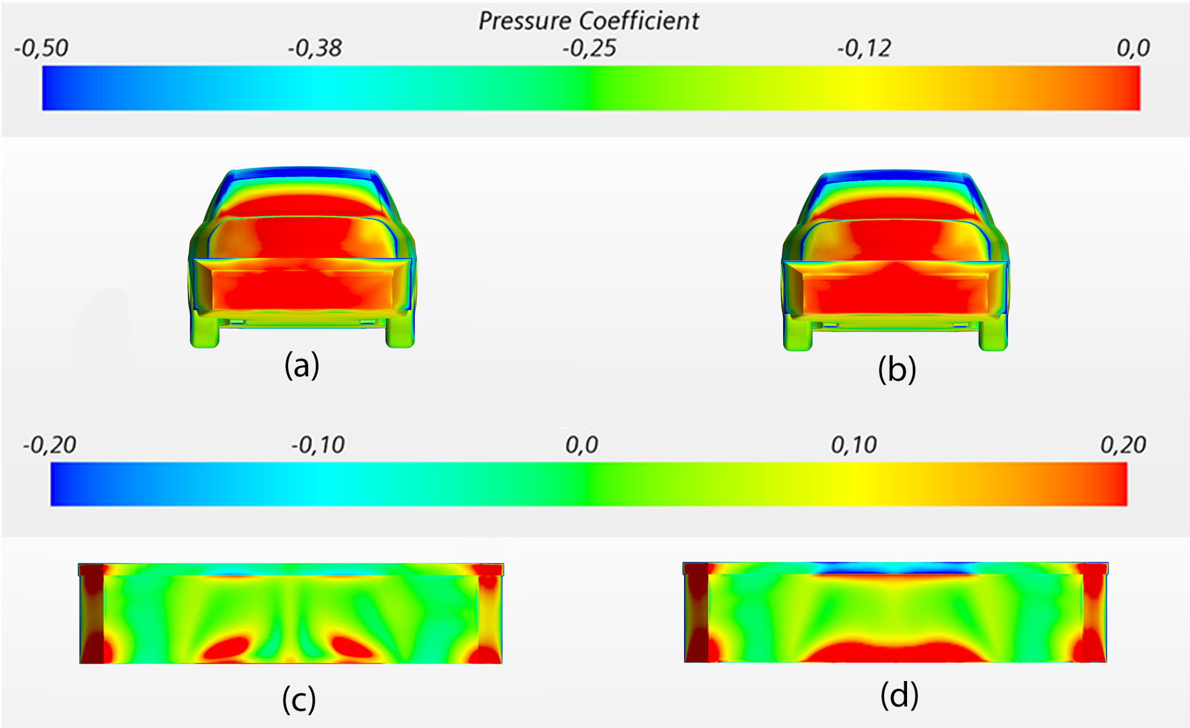

Figure 5.27: *Comparison of C_p on the surfaces of the car and IXTAbox. (a) is the improvement on the 170-40 box from behind (b) is the reference using 170-40 box from behind, (c) is the IXTAbox surface facing the car for the improvement on the 170-40 box, (d) is the IXTAbox surface facing the car for the reference using 170-40. The top color bar is for sub figure (a) and (b) while sub figure (c) and (d) use the middle color bar.*

When it comes to the stagnation point on the small extender, it can be seen to have the same geometric features as the large extender, and explains why the C_d difference between them is only 2 counts. With that in mind, it is proved that the most critical flow on the IXTAbox is the flow going from the underbody, stagnate on the IXTAbox surface to be mixed with the flow coming from the top.

5.6.3 Vortex Stabiliser

The *vortex stabiliser* is one of the aerodynamic devices that was inspired by the trucking industry rather than the car industry and proved to be a successful one in terms of reducing C_d. As previously discussed, the middle section of the box is where most of the flow from the underbody is flowing. Thus the distance between each baffle was not constant, instead, the distance in the middle was much shorter than the sides, which is observed in the appendix 7. By observation of figure 5.28 it can be seen that the improvement change the flow field compared to the reference case. When analysing the image in the symmetry plane, one can see that for the case of the improvement that the flow topology is a saddle, which is unique for this improvement and is likely due to the fact that the baffles influence the flow so that its angle to a vertical flow is smaller, than for the other devices tried. Thus it hits the flow from the top at a perpendicular angle which create the saddle topology, the creation sees this of a small rotating area closes to the trunk of the car. Moving on the the second wake plane 0.2m away from symmetry, no significant changes are observed when compared to the reference case, except for a slightly slower rotation between car and box.

The third plane to analyse does have some variations to it, where the flow coming from the side and separates seem to have a larger separation on the improved design compared to the reference case, likely due to higher static pressure on the side for the improved design as the flow is slower, thus a higher adverse pressure gradient.

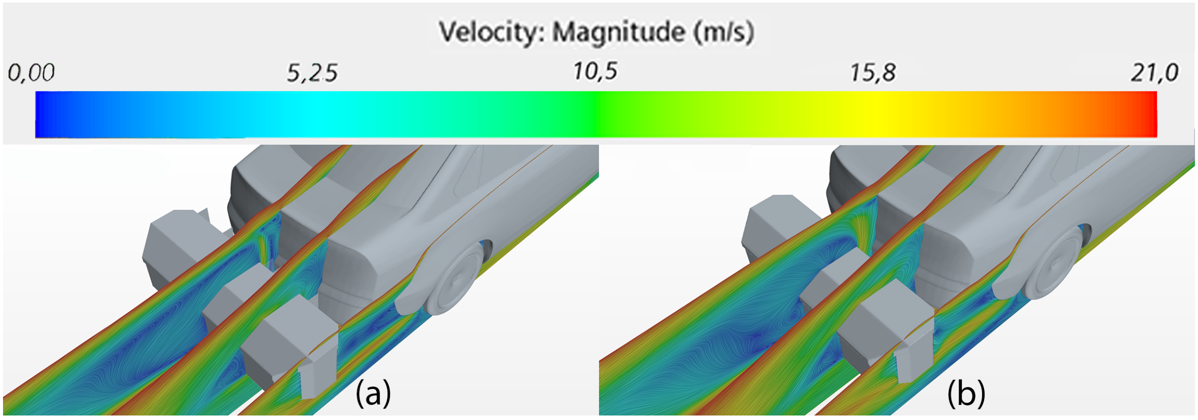

Figure 5.28: *Comparison of wake development for 3 XZ planes with Y values equal to [0,0.2,0.4] where image (a)is the improvement on the 170-40 box while image (b) is the 170-40 to be used as reference*

When analysing TKE as in figure 5.29 some of the conclusions drawn in the last image is further proved here. By looking at the improved design in figure 5.29 on can see that TKE is produced at the saddle point as the flow is rotating and turbulent in that section. On the other hand, TKE production where the flow from the underbody and top meets is significantly smaller for the improvement, likely because the baffles straighten the flow reducing the j component of the velocity vector in the volume between box and car. This reduction of the j component for the flow coming from the underbody induce less turbulence as one the flows are less chaotic.

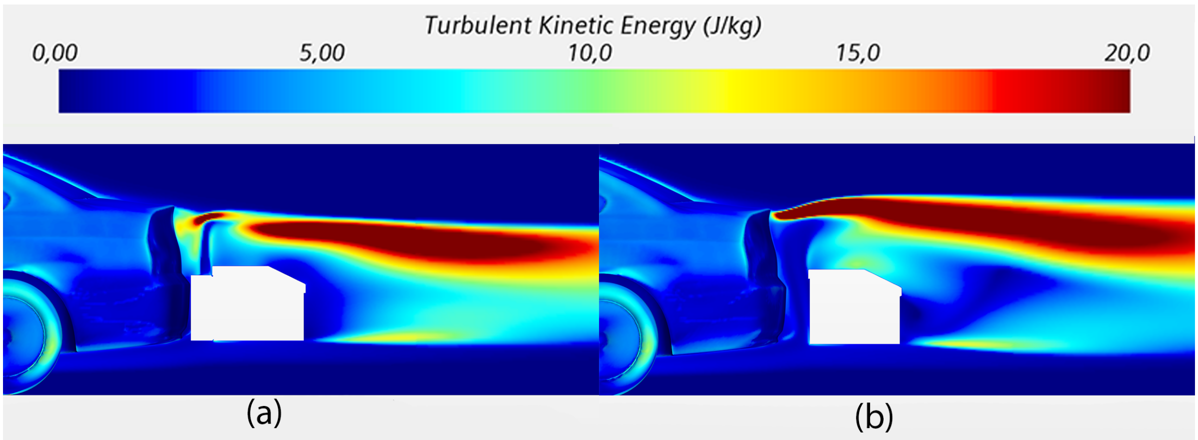

Figure 5.29: *Comparison of TKE for the XZ plane where Y=0 where image (a)is the improvement on the 170-40 box while image (b) is the 170-40 to be used as reference*

For the case of the pressure recovery on the trunk as seen in figure 5.30 it can be seen to decrease compared to the reference as the speed between box and car is higher compared to the reference. On the other hand the pressure recovery on the IXTAbox is higher than the reference aiding the reduction of C_dA.

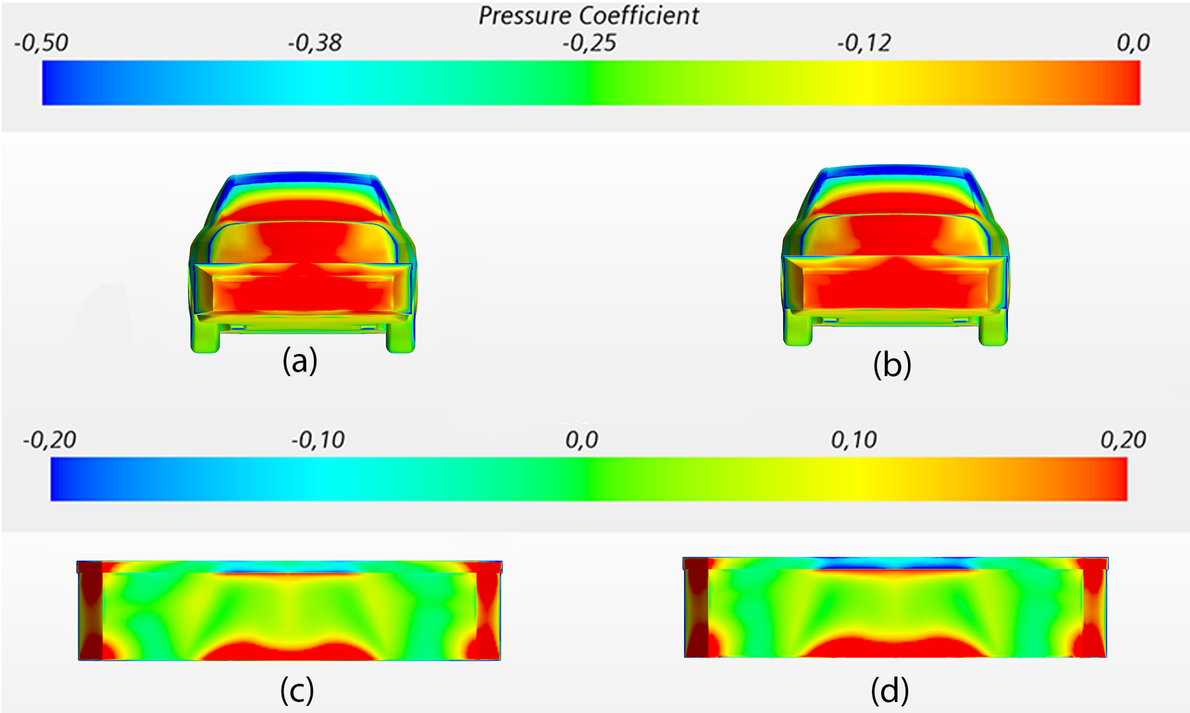

Figure 5.30: *Comparison of C_p on the surfaces of the car and IXTAbox. (a) is the improvement on the 170-40 box from behind (b) is the reference using 170-40 box from behind, (c) is the IXTAbox surface facing the car for the improvement on the 170-40 box, (d) is the IXTAbox surface facing the car for the reference using 170-40. The top color bar is for sub figure (a) and (b) while sub figure (c) and (d) use the middle color bar.*

The strength of the *vortex stabilizer* lies that it reduce the pressure a large percentage of the IXTAbox's surface facing the car. While it does not reduce the area where stagnation occur as for the diffuser extenders previously studied, it does reduce the base pressure or the other sections of the surface, indicated by its green teal colour rather than the green yellow color as for the reference in figure 5.30.

5.6.4 Arc Diffusor

The *arc diffusor* is the only improvement that is not focused on the flow coming from the underbody of the car that is shovelled by the box. Its purpose is to aid the separation that occurs for the flow that flows past the bottom of the IXTAbox, it will also help to balance the upwash compared to the downwash, as the IXTAbox removes the function of the diffusor on the car and creates an unbalanced upwash-downwash relationship.

In figure 5.31 which again shows three different planes of wake, one can see how the diffuser balances upwash and downwash better. In the reference case, a large vortex due to flow separation is observed behind the box for the symmetry plane, this vortex is rather large as the downwash is much stronger than the upwash. When implementing the diffusor, one can see how this vortex structure is reduced as the diffuser steer the flow upwards. Moving on to the other two planes in the same image, not many differences can be observed, which is reasonable as this improvement was the least efficient in terms of reducing C_d.

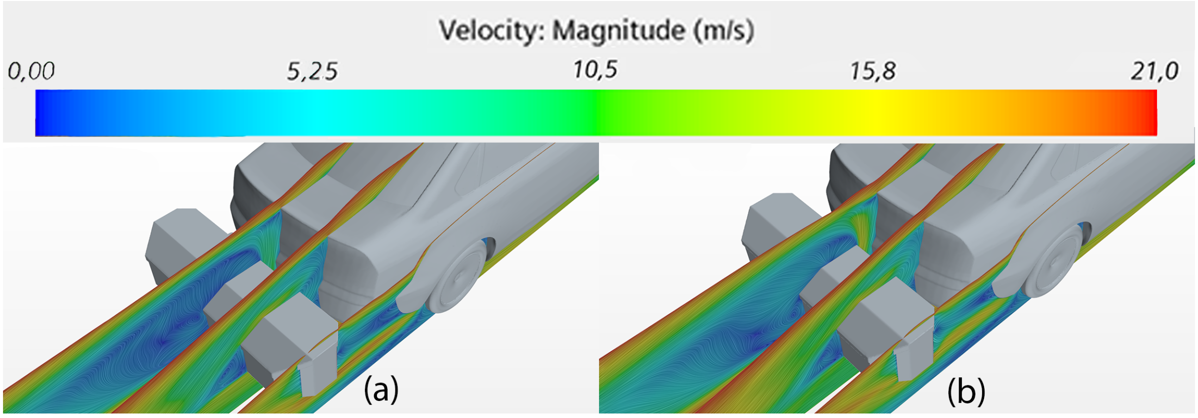

Figure 5.31: *Comparison of wake development for 3 XZ planes with Y values equal to [0,0.2,0.4] where image (a)is the improvement on the 170-40 box while image (b) is the 170-40 to be used as reference*

In figure 5.32 one can see that the intense TKE production for the top trailing edge is decreased, however for the diffusor it is due to re-balanced upwash downwash relationship, rather than changing the flow that goes between car and box. What is also observed is that the vortex diffusor have no influence on the volume between car and box, from which one could then conclude that the interference drag between an *arc diffusor* and *diffusor extension L* would be close to zero as they impact different parts of the flow, making in an exciting combo to further study.

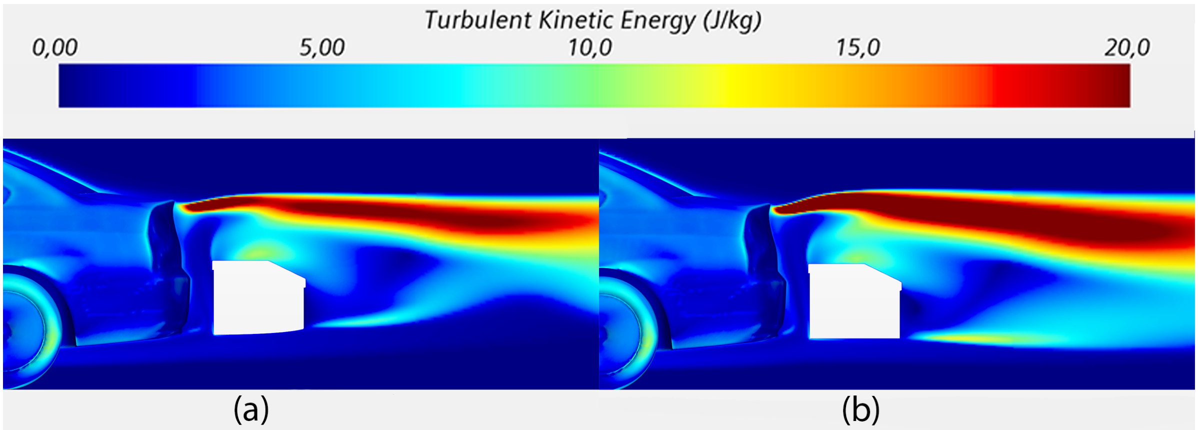

Figure 5.32: *Comparison of TKE for the XZ plane where Y=0 where image (a)is the improvement on the 170-40 box while image (b) is the 170-40 to be used as reference*

Apart from aiding the upwash downwash relationship, the diffusor also aid the flow separation from the bottom of the box. In the reference there is some turbulence produced for the flow leaving the bottom of the box. For the improvement however, the intensity and area of this TKE production is decreased, giving proof to a cleaner separation.

When it comes to the pressure recovery in figure 5.33 on the trunk between the arc diffusor and the reference, no difference can be seen. Some areas on the IXTAbox does have an increased pressure recovery compared to the reference, but are subtle. As expected the stagnation on the surface facing the car, show no difference what so ever as the improvement lies downstream of this area.

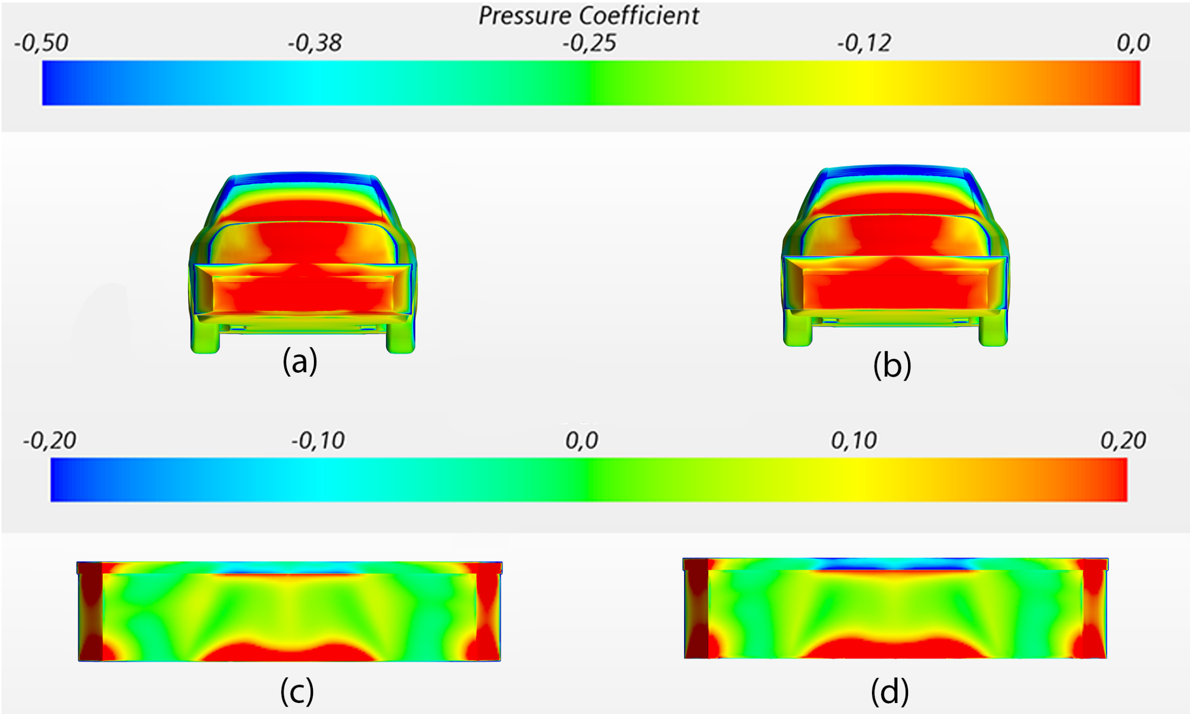

Figure 5.33: *Comparison of C_p on the surfaces of the car and IXTAbox. (a) is the improvement on the 170-40 box from behind (b) is the reference using 170-40 box from behind, (c) is the IXTAbox surface facing the car for the improvement on the 170-40 box, (d) is the IXTAbox surface facing the car for the reference using 170-40. The top color bar is for sub figure (a) and (b) while sub figure (c) and (d) use the middle color bar.*

6 Discussion

As no CFD studies can be found on objects in the wake of a car, and very little for roof boxes it is the *DrivAer* model that form the numerical validation and its quality in this thesis. The first validation is that of comparing C_d, in table 5.1 the reported values of C_d is observed to be *0.254*, *0,257* for respective turbulence model. From experimental studies, when using wind tunnels, a smooth underbody, notchback DrivAer has a C_d of *0.254*[17], the same study found C_d when using *CFD* with a one equation turbulence model to be *0.247*. The study do however have mirrors and handlebars which is not present in this thesis, though one can conclude that the numerical setup in terms of force monitors is very much a reasonable number. Moving on, the C_{ptot} wake plane 0.1m behind the car have been compared to the master thesis *Steady and Unsteady Numerical Analysis of the DrivAer Model* where it is concluded that their setup using RKE achieve a similar scalar plot[14] to the one presented in this thesis, the influence from the mirror in their wake could be seen which is of course not seen for this thesis. For the stated numbers above, aswell as fulfilling the convergence criterions in this thesis, the solutions shown are said to be accepted, except for the IXTAboxes of height 60 using RKE.

Reliable data on the impact on roof boxes is hard to find, the book *Aerodynamics of Vehicles* mention a 33% increase of C_d [8] for a roof box with luggage racks, but not much more information is given. For this reason, it was of interest to compare how two potential roof box models would compare, the results are reported in table 5.1. When comparing the reference only using the *DrivAer Notchback* to how the drag force increase when putting a roof box on top of the car, it is concluded that the adverse effects on the roof box is double-edged, as both the area and drag increase the power consumption significantly. By comparing the roof boxes to the reference, it can be seen that there are two primary reasons why C_d increase, the first reason is that the pressure recovery on the back window that could be seen for the car on its own, was negatively influenced by the roof box. The second reason is that it creates its own wake behind the box, as well as second stagnation point on the front of the box. Furthermore one can start to understand why roof boxes can pose a problem to the driver, it was discussed in section 3 on instabilities when using roof boxes. As the pressure on the surfaces of the car and a roof box change magnitude, the driving experience will be different compared to only using the car, as the direction of the force vectors acting on the car change. The drag force will likely increase the angle between the horizontal line as more wake is induced higher up on the test object, as well as the back window. Furthermore when introducing side winds, the moment will increase as the push occur at a much longer length away from the center of mass.

The IXTAbox on the other hand show no area increase for most cases as seen in table 5.1, while the increase of C_d is minimal. When comparing the wake of the IXTAbox compared to only using a car, some conclusions can be drawn. The IXTAbox affect the relationship between upwash and downwash rather drastically, affecting the pressure recovery on the box. The IXTAbox increase the base pressure on the car's trunk, and is a large reason why the increase of C_d is so small. The IXTAbox capture air from the underbody in all cases, while for the boxes of height 60, it also captures the flow from the sides and top of the trunk, however the two different turbulence models achieve different results on which flow is the strongest, e.g side flow, underbody flow or top flow. As the IXTAbox capture the flow mainly from the underbody, and steers it vertically to be mixed with the flow from the top, as seen in figure 5.20, stagnation occur on the box's surface facing the car making it the primary contributor to the drag increase of the IXTAboxes.

Moving on, it was found that RKE failed for the boxes of height 60 where an unsymmetrical solution of the wake was found, even while symmetry should be there. What is interesting is that the two first convergence criterions are fulfilled, namely residuals below 10^-4 and a force monitor variation below one for RKE. However, there is no reason why the solution should be asymmetric since the car and IXTAbox are mirrored in the symmetry plane, and a smooth underbody is used. At first, it was thought that i could be a meshing problem, however, the mesh in the wake is fine, have no orthogonality problems, but it was decided to decrease the mesh size even further so that roughly sixty million cells were tried, where another volumetric refinement around the box was added. This gave the same wrong solution, and it was deemed not to be the problem, then the y+ values on the IXTAbox was increased to see if that could be the problem since some small sections are a bit too small where the velocity is low. However, no change was seen, thus after some time of troubleshooting and reading up on theory, it was found that RKE can have problems when modelling adverse pressure gradients. When it comes to vehicle aerodynamics, adverse pressure gradients are found when the fluid decelerates after the car's largest cross-section. $k-\omega$ however, handles adverse pressure gradients better [4] but are harder to find appropriate boundary conditions to, to mitigate this, the SST addition was deemed appropriate. When using $k-\omega$ there was always flow coming from the underbody, up along the vertical line between box and car, and C_d values were more reasonable.

When analyzing $k-\omega$, it should also be carried out critically as it is not deemed to be a perfect solution. The residuals and force monitor fulfil the convergence criterions, but show periodicity, which could indicate that the solution has a hard time finding a steady-state. This periodicity, while being common together with the fact that RKE fails leads to the recommendation that this study should be verified using a transient solver and potentially wind tunnel.

Moving on to the height variation study, which was conducted to observe how the flow is affected by lowering the IXTAbox, which is something that can be done by the user, it was seen that the intensity of the flow shovelling is increased. This indicates that height is a sensitive parameter, eg how much flow the box captures from the underbody flow and influenced the approach to the aerodynamic improvements. Furthermore, it was seen that while decreasing the height in constant intervals, the increase of C_d was far from linear, which indicate a critical point in the relationship between the shape and height of the diffusor to the height of the IXTAbox above ground. It should also be pointed out here that the height variation study shows that the relationship between the diffusor on the car and the IXTAbox is important, while the general conclusions drawn from the thesis could be applied to other car models, care should be taken nevertheless as an diffusor with a sharp angle will allow more flow to hit the IXTAbox, increasing the stagnation that occur on its face, facing the car, increasing C_d.

To finalize the study, a large part of the time was spent to investigate aerodynamic improvements to the IXTAbox. The goal of this thesis is to study how the wake changes when introducing an object to the wake and study which parameters are sensitive. The three most successful aerodynamic improvements share one quality, they reduce the pressure on the IXTAbox's surface facing the car, either by removing the stagnation point, or by reducing the base pressure where no stagnation occur. The arc diffusor on the other hand aid the upwash-downwash relationship which is affected as the IXTAbox cover the diffusor on the car. The improvements that did very little to change C_d were found through analysis of TKE. While they decreased turbulence in the area, they were supposed to decrease turbulence, they introduced more turbulence in other areas through interference. Due to the time limit, they have not been as extensively studied as the improvements that did positively impact C_d, and important qualities of them could have been missed, such as putting the same aerodynamic device on another IXTAbox than the 170-40 box.

7 Conclusions

From wrapping up the thesis, some suggestions on future work shall be made. First, an unsteady solver should run the cases, especially for the large 60 boxes, as they have been shown to be problematic with the steady solver. Furthermore, a study on side winds should be conducted in order for the model to become closer to a real road case.

The purpose of this study has been to investigate if the IXTAbox could play a part in mitigation of CO_2 emissions. It has been shown that IXTAboxes are a great way to decrease the negative impact to the energy efficiency when extra luggage capacity is required as the power increase is drastically lower compared to a roof box.

The drag penalty compared to the *DrivAer* model on its own is largely attributed to the stagnation that occurs on the IXTAbox surface, facing the car. For that reason it was found that sensitive parameters to the increase of C_dA is both the height above the ground, as well as the size of the IXTAbox. Furthermore, an important note should be made that the box also helps the pressure recovery on the trunk of the car which is why C_d is only increasing by a few % compared to *DrivAer*. With that in mind, a mapping study have been carried out where typical aerodynamic devices have been tried out on the IXTAbox where 3 improvements achieved a lower C_dA value than *DrivAer* on its own making the IXTAbox a very interesting product for further study.

References

[1] James R. Welty, Charles E. Wicks, Robert E. Wilson, and Gregory L. Rorrer, *Fundamentals of Momentum, Heat, and Mass Transfer*, 5th ed. New York: Wiley, 2007.

[2] Oliver Cleynen, *Boundary layer separation.* [Online]. Available: `https://en.wikipedia.org/wiki/Flow_separation#/media/File:Boundary_layer_separation.svg`.

[3] Aakash30jan, *Energy Cascade.*

[4] Bengt Andersson, Ronnie Andersson, Love Håkansson, Mikael Mårtensson, Rahman Sudiyo, and Berend van Wachem, *Computational Fluid Dynamics for Engineers*, 14th ed. Göteborg: Cambridge University Press, 2018.

[5] Dr Mesh, Ed., *Detached eddy simulation*, Jan. 2021. [Online]. Available: `https://en.wikipedia.org/wiki/Detached_eddy_simulation`.

[6] D. C. Wilcox, *Turbulence modeling for CFD.* DCW Industries, 2006, p. 522, ISBN: 1928729088.

[7] E. Josefsson, "Examination of robustness and accuracy of CFD simulations for external aerodynamics of commercial vehicles," Applied Mechanics, Göteborg, Tech. Rep., 2019.

[8] THOMAS CHRISTIAN SCHUETZ., *AERODYNAMICS OF ROAD VEHICLES.* SAE SOC OF AUTOMOTIVE ENG, 2016, ISBN: 9780768082531.

[9] Sebben Simone, *MTF236 Road Vehicle Aerodynamics Post-Processing in Vehicle Aerodynamics*, Göteborg, 2021.

[10] S. O. Kang *et al.*, "A study of an active rear diffuser device for aerodynamic drag reduction of automobiles," *SAE Technical Papers*, SAE International, 2012. DOI: `10.4271/2012-01-0173`.

[11] U. Akta and K. Abdallah, "Aerodynamics Concept Study of Electric Vehicles Drag Reduction and Range Increase," Applied Mechanics, Göteborg, Tech. Rep., 2017.

[12] R. M. Janicki and A. Piechna, "Examining influence of a rooftop cargo carrier position on automobile aerodynamics," *AIP Conference Proceedings*, vol. 2078, American Institute of Physics Inc., Mar. 2019, ISBN: 9780735418066. DOI: `10.1063/1.5092076`.

[13] G. Lundegaard Lange, "External Aerodynamic Optimization of Ground Vechicles using the Adjoint Method," Applied Mechanics, Göteborg, Tech. Rep., 2021.

[14] R. Yazdani, "Steady and Unsteady Numerical Analysis of the DrivAer Model," Applied Mechanics, Göteborg, Tech. Rep., 2015.

[15] *Star-CCM+ Documentation*, 2021. [Online]. Available: `https://docs.sw.siemens.com/documentation/external/PL20200805113346338/en-US/userManual/userguide/html/index.html#page/STARCCMP%2FGUID-70D648E4-1172-43E5-8F45-C8D92F12D814.html%23`.

[16] J. Cho, J. Park, K. Yee, and H. L. Kim, Comparison of Various Drag Reduction Devices and Their Aerodynamic Effects on the DrivAer Model, *SAE International Journal of Passenger Cars - Mechanical Systems* **11**, no. 3 Jul. 2018, 225–238, Jul. 2018, ISSN: 19464002. DOI: `10.4271/06-11-03-0019`.

[17] D. Wieser, H. J. Schmidt, S. Müller, C. Strangfeld, C. Nayeri, and C. Paschereit, Experimental Comparison of the Aerodynamic Behavior of Fastback and Notchback DrivAer Models, *SAE International Journal of Passenger Cars - Mechanical Systems* **7**, no. 2 2014, 682–691, 2014, ISSN: 19464002. DOI: `10.4271/2014-01-0613`.

Appendix

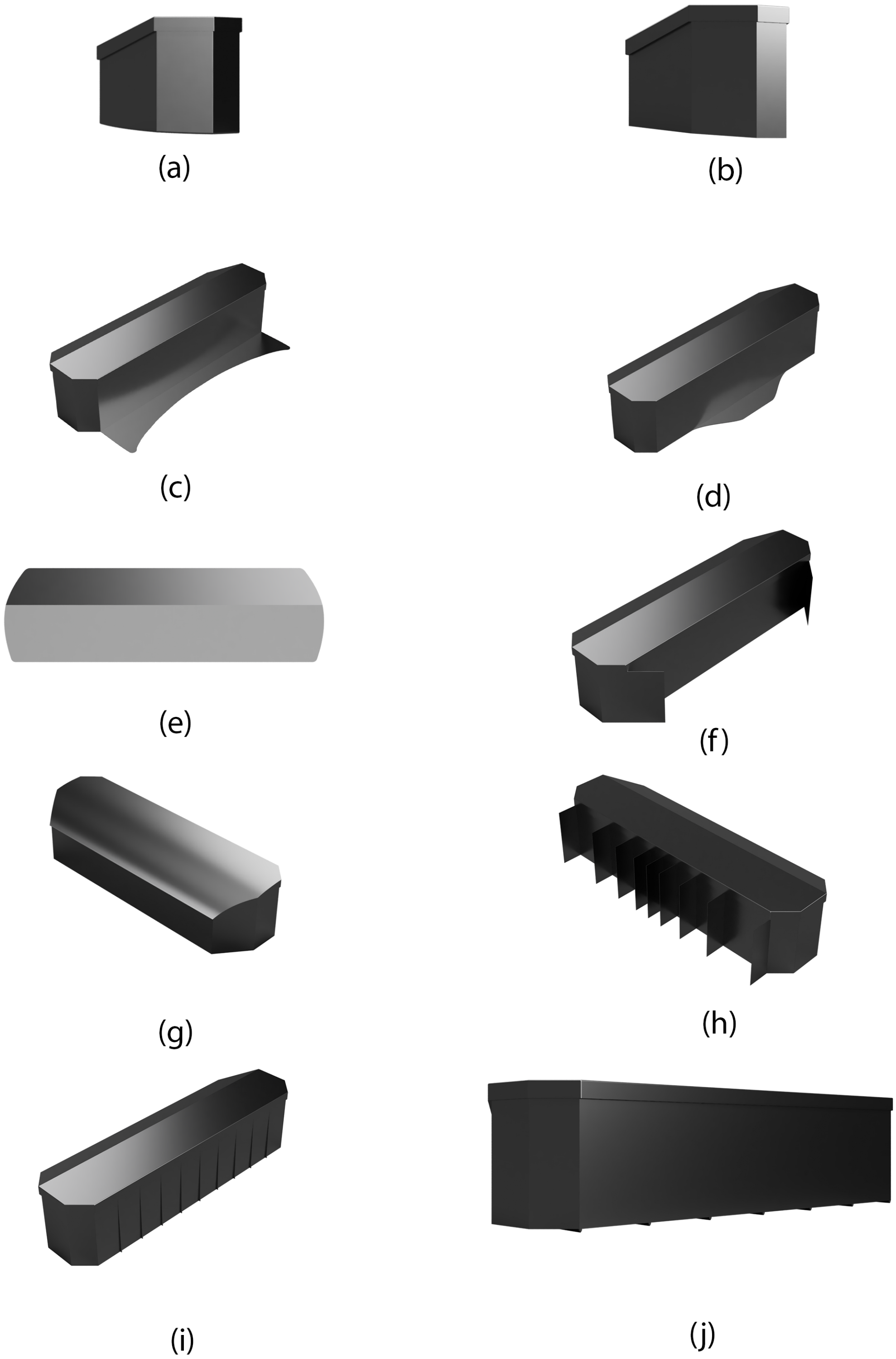

Figure A.1: *(a) Arc diffusor, (b) Straight diffusor, (c) Large diffuser extender, (d) Small Diffuser extender, (e) Rounded edge, (f)Side panels 20 cm, (g) Tear drop top, (h) Vortex Stabiliser, (i) Z-baffles, (j) X-baffles*

DEPARTMENT OF Mechanics and Maritime Sciences
CHALMERS UNIVERSITY OF TECHNOLOGY
Gothenburg, Sweden 2022
www.chalmers.se

CHALMERS
UNIVERSITY OF TECHNOLOGY